# Theoretical and Spectroscopic Studies of Tetrahedral Clusters of the Type $[L_3M(\mu\text{-}H)_x\{AuL'\}_3]^{2+}$ (M = Rh, Ir, $x$ = 2; M = Ru, $x$ = 3)

**Alberto Albinati,[1a] Jürgen Eckert,[1b] Peter Hofmann,[1c] Heinz Rüegger,[1d] and Luigi M. Venanzi*[,1d]**

Istituto di Chimica Farmaceutica, Università di Milano, I-20131 Milano, Italy, LANSCE, Los Alamos National Laboratory, Los Alamos, New Mexico 87545, Anorganisch-chemisches Institut der Technischen Universität München, D-8046 Garching, Germany, and Laboratorium für Anorganische Chemie, ETH-Z, CH-8092 Zürich, Switzerland

*Received August 4, 1992*

The structural and bonding aspects of the hydride ligands in the cationic clusters $[(triphos)MH_2\{Au(PPh_3)\}_3]^{2+}$ (triphos = $CH_3C(CH_2PPh_2)_3$; M = Rh and Ir) and $[(triphos)RuH_3\{Au(PPh_3)\}_3]^{2+}$ were investigated by a variety of techniques. The $^{31}$P-CP-MAS spectra (162 MHz) of the clusters $[(triphos)MH_2\{Au(PPh_3)\}_3](CF_3SO_3)_2$ (M = Rh and Ir), $[(triphos)RuH_3\{Au(PPh_3)\}_3][PF_6]_2$, and $[(triphos)RuH_2\{Au(PPh_3)\}_3][PF_6]$ show that in the dihydrido complexes the phosphorus atoms of the triphos ligands, as well as those of the $PPh_3$ molecules, are inequivalent while the corresponding donors in the *trihydrido complex* are equivalent. The $^{197}$Au Mössbauer spectra of the rhodium and iridium complexes show that two of the gold atoms in the dihydrido clusters are different from the third. Furthermore, the values of the isomer shifts and quadrupole splittings indicate that the bridging hydride ligands are best described as being intermediate between $\mu_2$ and $\mu_3$ (quasi-$\mu_3$). Incoherent inelastic neutron spectroscopic (IINS) and IR studies of the rhodium and ruthenium clusters were carried out to unambiguously assign the M–H vibrational modes. These spectra show bands at ca. 1600 cm$^{-1}$ (assigned to $\nu_{as}$(M–H–Au) that exclude a pure $\mu_3$ bridging mode for the hydride ligands but are consistent with a quasi-$\mu_3$ model. Finally MO model calculations of the extended Hückel type for $[(PH_3)_3Rh(AuPH_3)_3](H)_3^{3+}$, $[(PH_3)_3Rh(AuPH_3)_3](H)_2^{2+}$, and $[(PH_3)_3Rh(AuPH_3)_3](H)^+$, which served as simplified models of real hydrido cluster cations, have been performed. A general bonding scheme is presented, analyzing electronic and molecular structures for this class of compounds, including the question of possible hydride locations, on the basis of a transparent fragment orbital (FMO) description and by means of various geometry optimization calculations. The theoretical results are in accord with spectroscopic data and allow their consistent interpretation. Thus, all these studies are in agreement with a quasi-$\mu_3$ structure for the hydride ligands in these clusters.

## Introduction

During recent years the development of rational and planned synthetic procedures to generate mixed-metal gold clusters has provided access to a variety of such species, neutral or ionic, and is presently leading to a rapidly expanding knowledge in this area of chemistry.[2] Of particular interest are those heterometallic gold clusters that also contain hydride ligands, because there exists a well-established isolobal analogy between $H^+$ and the $AuL^+$ cations, which are often used as building blocks in such molecules.[3] Therefore, mixed-metal gold hydride clusters, apart from having potential relevance with respect to homogeneous or heterogeneous catalysis,[4] pose highly challenging questions related to bonding/structure relationships, spectroscopy, and structural dynamics (fluxionality).

Recently Venanzi and co-workers reported the synthesis of a series of novel hydrido-bridged cationic gold–rhodium, gold–iridium,[5] and gold–ruthenium clusters[6] obtained by reacting the trihydrides [(tripod)$MH_3$] (M = Rh, Ir; tripod = $CH_3C(CH_2EPh_2)_3$ with E = P (triphos) or As (triars)) or related ruthenium precursor complexes with gold(I) phosphine and arsine $AuL^+$ cations. Depending upon experimental conditions, cationic hydrido clusters with one, two, or three AuL units (L = phosphine, arsine) were isolated and fully characterized.

Especially intriguing are those cases where three AuL fragments and one (tripod)M subunit form a tetrahedral $MAu_3$ framework, which, according to analytical, spectroscopic, and structural data, additionally incorporates two or three hydride ligands and carries an overall +2 or +1 charge. X-ray structure analyses on the three isostructural compounds $[(triphos)RhH_2\{Au(PPh_3)\}_3](CF_3SO_3)_2$,[5] **[1]**$(CF_3SO_3)_2$, $[(triphos)IrH_2\{Au(PPh_3)\}_3][PF_6]_2$,[5b] **[2]**$[PF_6]$, and $[(triphos)RuH_3\{Au(PPh_3)\}_3][PF_6]_2$,[6] **[3]**$[PF_6]_2$, were carried out confirming the metallotetrahedrane skeletal arrangement. It should also be noted that the rhodium and iridium cluster triflates are isomorphous with the corresponding hexafluorophosphates.

Some unusual spectroscopic and structural features of these $MAu_3$ tetrahedral clusters, related to the location and possible mobility of the hydride ligands, as well as to general cluster fluxionality and bonding problems, deserve attention. Thus the crystal structure determinations of the dihydrides **1**–**3** show that these dications lie on a crystallographic 3-fold axis going through the $CH_3$–C bond of triphos, M (M = Rh, Ir, Ru), and the midpoint of the $Au_3$ triangle. Thus, all M–Au, Au–Au, M–P, and Au–P distances are equal. A summary of the relevant cluster bonding parameters is given in Table I. The positions of the bridging hydride ligands in the ruthenium cation **3** were found on the Fourier map and could be refined.

(1) (a) Università di Milano. (b) Los Alamos National Laboratory. (c) Technische Universität München. (d) ETH Zürich.
(2) Hall, K. K.; Mingos, D. M. P. *Prog. Inorg. Chem.* **1984**, *32*, 237 and references quoted therein.
(3) (a) Evans, D. G.; Mingos, D. M. P. *J. Organomet. Chem.* **1982**, *232*, 171. (b) Hoffmann, R. *Angew. Chem.* **1982**, *94*, 725; *Angew. Chem., Int. Ed. Engl.* **1982**, *21*, 711. (c) Lavigne, G.; Papageorgiou, F.; Bonnet, J.-J. *Inorg. Chem.* **1984**, *23*, 609 and references quoted therein. (d) Mingos, D. M. P. *Polyhedron* **1984**, *3*, 1289.
(4) (a) Braunstein, P.; Rose, J. In *Stereochemistry of Organometallic and Inorganic Compounds*; Bernal, I., Ed.; Elsevier: Amsterdam, 1980; Vol. 3. (b) Clark, H. C.; Jain, V. K. *Coord. Chem. Rev.* **1984**, *55*, 151.
(5) (a) Albinati, A.; Demartin, F.; Janser, P.; Rhodes, L. F.; Venanzi, L. M. *J. Am. Chem. Soc.* **1989**, *111*, 2115 and references quoted therein. (b) Albinati, A. Personal communication.
(6) (a) Albinati, A.; Venanzi, L. M.; Wang, G. *Inorg. Chem.*, in press. (b) Wang, G. Dissertation, ETH Zürich, No. 9398, 1991.

0020-1669/93/1332-2377$04.00/0 

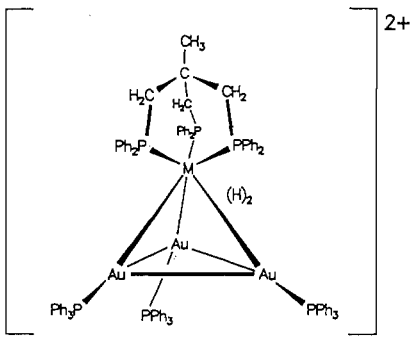

*1 : M = Rh; 2 : M = Ir*

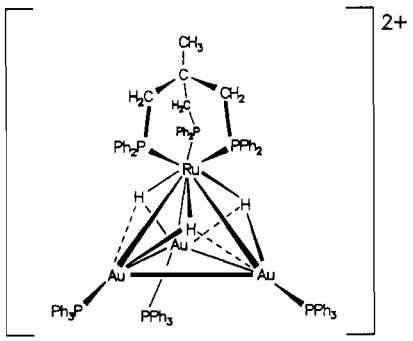

*3*

In the ruthenium cation, with its three hydride ligands, the imposed crystallographic symmetry corresponds to the molecular symmetry.[6] Due to the uncertainties in the locations of the hydride ligands, it is not possible to reliably describe their bridging mode as either $\mu_2$ or $\mu_3$. However, the structural data, taken in conjunction with the spectroscopic results and the theoretical calculations (see later), are best interpreted in terms of an intermediate situation which will be referred to as quasi-$\mu_3$. In this case molecular symmetry will be lower than $C_{3v}$ even though the $C_3$ axis is preserved.

However, problems arise in assigning a static molecular structure to the rhodium and iridium complexes where the presence of only *two hydride ligands*, which could not be located on the Fourier maps, could lower the molecular symmetry. In fact, there is one hydride arrangement which gives a cluster with a crystallographic $C_3$ axis, i.e., that in which one hydride is inside the $MAu_3$ tetrahedron and the other caps the triangular $Au_3$ face. Although this structure may appear to be unlikely, it cannot be discarded a priori on the basis of the available X-ray data. However, as will be shown later, MO calculations indicate that such an arrangement would have very high energy. Thus, careful examination of the crystal structure is needed to establish whether the observed crystallographic symmetry is the result of disorder.

In this case there are two possible explanations for the apparent equivalence of the three $MAu_2$ faces: (1) a *static disorder* in which the random distributions of the cations, which do not have $C_3$ symmetry, gives rise to average symmetry consistent with the crystallographic $C_3$ axis and (2) a *dynamic disorder* caused by the fluxional behavior of the hydride ligands on the cluster faces (dynamic averaging).

Furthermore, any consideration of such disorder must also take into account the common feature of M–M bonds, i.e., that they lengthen upon formation of the corresponding M–H–M moieties.[7]

In choosing between these two alternatives, one must also take into account that there are no unusual features in the anisotropic displacement parameters of **1** (or **2**) relative to **3** as the mean-square amplitudes of vibration for the two structures are almost identical (see Figure 1 and Table II) and fall between 0.15 [5] and 0.28 Å.[6] Therefore, a superimposition of *significantly* different Rh–Au and Au–Au vectors is ruled out by the magnitude and orientation of the ellipsoids. However, the crystal data cannot exclude a static disorder if the differences in Rh–Au and Au–Au distances are *smaller* than ca. 0.025 Å.

**Table I.** Selected Distances (Å) in Cations $[(triphos)MH_2\{Au(PPh_3)\}_3]^{2+}$ (M = Rh, **1**, M = Ir, **2**) and $[(triphos)RuH_3\{Au(PPh_3)\}_3]^{2+}$, **3**

| | M = Rh (**1**)[5a] | M = Ir (**2**)[5b] | M = Ru (**3**)[6] |
|---|---|---|---|
| M–Au | 2.695(2) | 2.693(3) | 2.679(2) |
| Au–Au | 2.887(1) | 2.882(2) | 3.003(1) |
| M–P | 2.313(5) | 2.29(9) | 2.330(5) |
| Au–P | 2.260(5) | 2.27(1) | 2.326(5) |
| M–H | n.o. | | 1.9(2) |
| Au–H | n.o. | | 1.7(2) |
| Au′–H | n.o. | | 2.6(2) |

Furthermore, the above considerations induce one to give serious consideration to a possible dynamic averaging resulting from site exchange of the hydride ligands on the cluster faces as this type of behavior has been found in solution.[8] While the $^{31}P$ and $^{1}H$ NMR spectra of **1** at temperatures below ca. −50 °C are consistent with a structure such as **1a**, at room temperature, the phosphorus nuclei of triphos are magnetically equivalent, as are the phosphines on gold.[5] This implies a site exchange of the hydride ligands relative to the $Au_3$ and triphos frameworks. Furthermore, NMR studies of the $RhAu_3$ clusters in which triphos has been replaced by the ligands *RRR/SSS*-triphos*, **4a**, and *RRS/SSR*-triphos*,

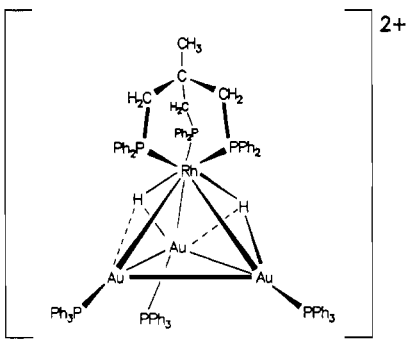

*1a*

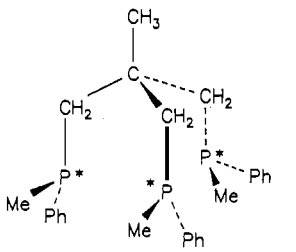

*4a*

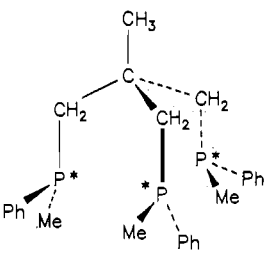

*4b*

**4b**,[8] i.e., $[(triphos^*)RhH_2\{Au(PPh_3)\}_3](CF_3SO_3)_2$ (triphos* = *RRR/SSS*- or *RRS/SSR*-triphos*), show the existence of three dynamic processes which are best detected in the complex with the latter ligand: (a) rapid rotation of the trigold moiety relative to the (triphos*)$RhH_2$ unit; (b) mutual exchange of the diastereotopic hydrides; (c) slow rotation of the *RRS/SSR*-triphos* unit in the diastereoisomer. While the first and last of these processes cannot occur in the solid state, the second could well be operative.

(7) Kaesz, H. D. *Chem. Brit.* **1973**, *9*, 344.

(8) Imhof, D.; Rüegger, H.; Venanzi, L. M.; Ward, T. R. *Magn. Reson. Chem.* **1991**, *29*, 573.

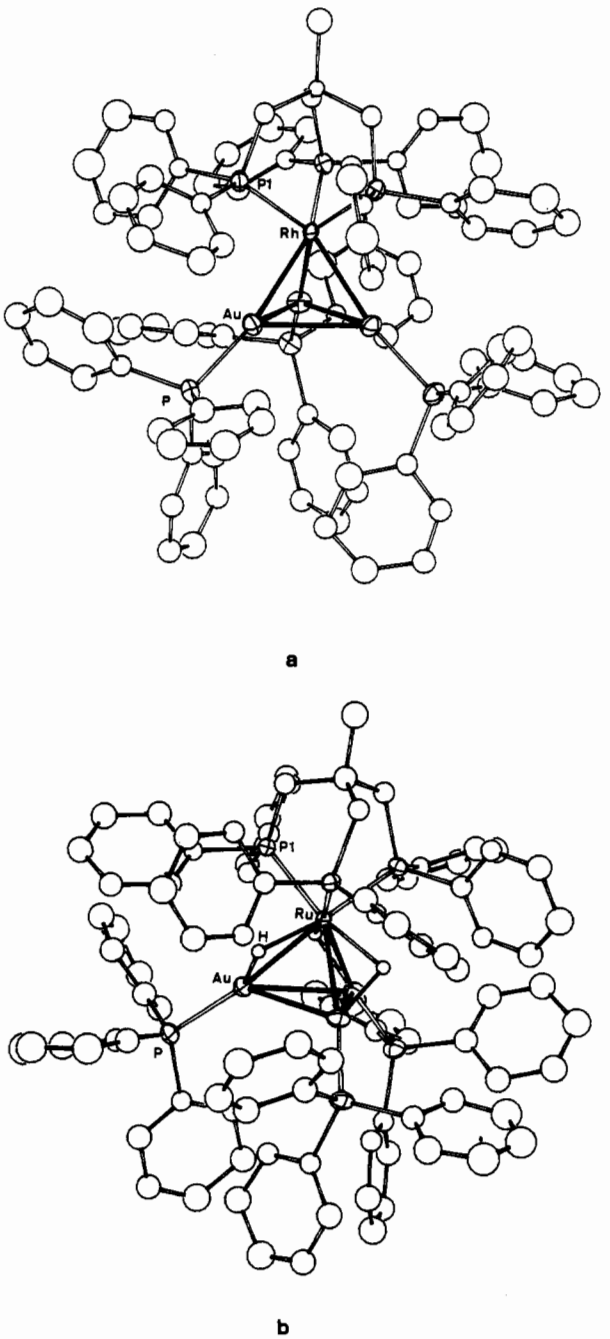


**Figure 1.** ORTEP views of the cations (a) $[(triphos)RhH_2\{Au(PPh_3)\}_3]^{2+}$, **1**, and (b) $[(triphos)RuH_3\{Au(PPh_3)\}_3]^{2+}$, **3**.

**Table II.** Root-Mean-Square Amplitudes of Anisotropic Displacements (Å) of the Heavy Atoms in the Cations $[(triphos)RhH_2\{Au(PPh_3)\}_3]^{2+}$, **1**, and $[(triphos)RuH_3\{Au(PPh_3)\}_3]^{2+}$, **3**

| | M = Rh (1)[5] | | | M = Ru (3)[6] | | |
|---|---|---|---|---|---|---|
| | min | interm | max | min | interm | max |
| M | 0.12 | 0.17 | 0.28 | 0.15 | 0.16 | 0.19 |
| Au | 0.18 | 0.22 | 0.28 | 0.17 | 0.20 | 0.25 |
| P(1) | 0.18 | 0.23 | 0.25 | 0.16 | 0.21 | 0.26 |
| P(2) | 0.17 | 0.19 | 0.22 | 0.17 | 0.18 | 0.20 |

These observations, in connection with the well-known mobility of hydrogen on cluster faces, could be taken to indicate that the apparently symmetric cluster geometry observed for **1**, *in the solid-state structure* (vide supra), might not originate from static hydride locations on the $C_3$ axis (e.g., interstitial and capping) but rather be caused by a rapid site exchange of the two hydrides among either the three equivalent $RhAu_2$ faces or Rh–Au edges.

There have been only two previous reports in the literature of closely related $MAu_3$ gold tetrahedranes, i.e., $[(PMePh_2)_3ReH_3\{Au(PPh_3)\}_3][BF_4]$,[9] **[5]**$[BF_4]$, and $[(PPh_3)_2(CO)RhH\{Au(PPh_3)\}_3][PF_6]$,[10] **[6]**$[PF_6]$. Both monocations are isoelectronic with **1** and **3**.

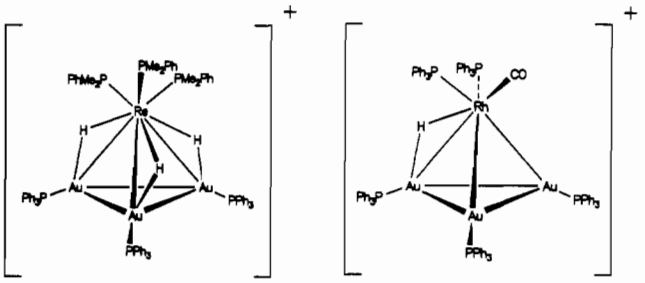


*5* *6*

Interestingly, the X-ray crystal structure of the $ReAu_3$ system **5** shows that the $P_3Re(AuP)_3$ moiety adopts a nearly eclipsed conformation. On the basis of molecular mechanics (potential energy calculations) and from Fourier difference maps, the three hydrides were assigned positions almost exactly trans to the Re–P vectors and were interpreted as being in an edge-bridging Re-($\mu_2$-H)Au bonding mode. In fact, given the reported, nearly eclipsed, relative orientation of the $ReP_3$ fragment with respect to the $Au_3$ triangle, a trans position of the hydrides to the Re–P bonds automatically implies a quasi-$\mu_3$ bridging arrangement of the hydrides. Structural data for **6** show a nearly staggered conformation of the core atoms, one Rh–Au bond, that trans to the CO ligand, being significantly longer than the others. On this basis a $\mu_2$-hydride bridging this bond has been considered as most probable, although in this compound the unsymmetric set of ligands at rhodium per se must lead to inequivalent Rh–Au bonds and consequently to some distortion of the $RhAu_3$-cluster frame.

The available data for **1** do not allow a reliable structural assignment of the minimum energy positions for the two hydrides. Although, as mentioned earlier, NMR experiments allow a detailed description of the dynamic processes in solution, the question of the hydride position in the "frozen", static structure ($\mu_2$ vs $\mu_3$), at the low-temperature limit, remains still open and the same is true for the solid state.

If we make the reasonable assumption that bridging geometries in Rh–H–Au and Ru–H–Au are similar, then, due to the shorter Au–Au separation in **1**, the bridging hydrides in the former complex could be expected to have more $\mu_3$ character than in the corresponding ruthenium species.

In order to clarify the uncertainties mentioned above, solid-state $^{31}P$ NMR, $^{197}Au$ Mössbauer and incoherent inelastic neutron scattering (IINS) spectroscopic studies, as well as EH–MO model calculations, were carried out and are described below.

## Solid-State NMR Spectroscopy

NMR spectroscopy, performed on compounds in the solid state, provides a valuable link between their molecular geometry in that phase, derived from X-ray crystallography, and the structural information obtained for the same species from solution NMR data. As the positions of the signals in an NMR spectrum are mostly determined by the *local* electronic environment of the nuclei, the picture obtained reflects the symmetry of the individual molecules as opposed to the information provided by X-ray crystallography, which mirrors the relative arrangement of a large number of molecules imposed by the symmetry of elements of the crystal. This difference can be very important when the crystal symmetry is higher than the molecular symmetry as, in such a

(9) Sutherland, B. R.; Folting, K.; Streib, W. E.; Ho, D. M.; Huffman, J. C.; Caulton, K. G. *J. Am. Chem. Soc.* **1987**, *109*, 3489.
(10) Boyle, P. D.; Johnson, B. J.; Buehler, A.; Pignolet, L. H. *Inorg. Chem.* **1986**, *25*, 5.

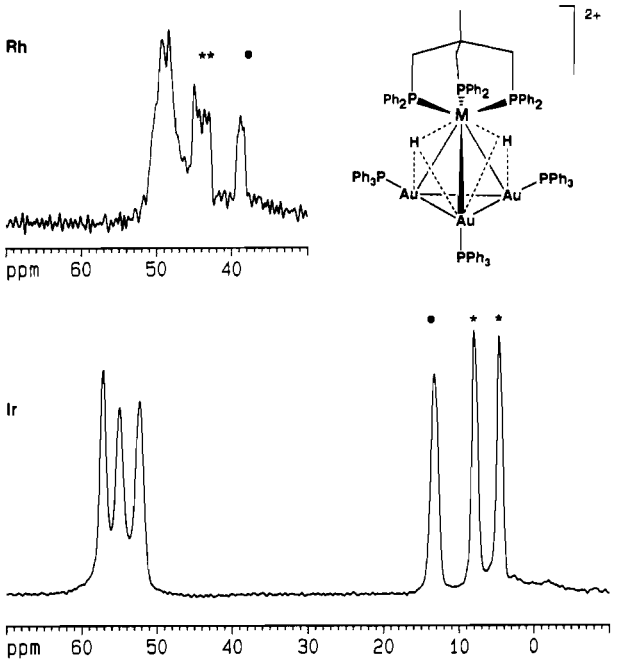


**Figure 2.** $^{31}$P-CP-MAS spectra (162 MHz) of [(triphos)-$MH_2\{Au(PPh_3)\}_3](CF_3SO_3)_2$: M = Ir (lower trace), [**2**]$(CF_3SO_3)_2$; M = Rh (upper trace), [**1**]$(CF_3SO_3)_2$. The triphos resonances are marked with asterisks.

case, the geometry derived from the X-ray data corresponds to the "real" geometry averaged out by the symmetry operations of the crystal. However, solid-state NMR spectroscopy "sees" the "true" molecular symmetry and one obtains a spectrum which is largely determined by the actual molecular geometry because (1) the individual molecules are identical and (2) the disorder has only a minor influence on the pattern of resonances.

When evaluating solid-state NMR spectra, one should take into account that the lower mobility of groups within molecules, which is characteristic of condensed matter, results in an environment in which the symmetry of the NMR-active nuclei is lower than that present in solution where dynamic averaging generally occurs. Thus additional signals can be observed in the solid-state spectra.

As mentioned earlier, a static disorder might be present in crystalline [(triphos)$MH_2\{AuPPh_3\}_3](CF_3SO_3)_2$ (M = Rh, [**1**]$(CF_3SO_3)_2$, and Ir, [**2**]$(CF_3SO_3)_2$). Thus solid-state NMR spectra, e.g., $^{31}$P, were recorded to obtain information about the molecular symmetry in these complexes and, therefore, on the possible locations of the hydride ligands. It should be recalled here that these compounds are isostructural[5b] and give fully analogous $^1$H and $^{31}$P NMR spectra in solution.[5a]

As the interpretation of the $^{31}$P solid-state NMR spectrum of [**1**]$(CF_3SO_3)_2$ is not straightforward, the spectrum of the corresponding iridium complex [(triphos)$IrH_2\{Au(PPh_3)\}_3](CF_3SO_3)_2$, [**2**]$(CF_3SO_3)_2$, will be discussed first.

The $^1$H-decoupled $^{31}$P-spectrum of the above iridium complex *in solution*, at room temperature, is consistent with an $A_3X_3$ spin system and, therefore, with the equivalence of (1) the three phosphorus spins of triphos and (2) those of the three $PPh_3$ molecules. This can be attributed to dynamic averaging arising from fast rotation of both the triphos ligand and the $\{AuPPh_3\}_3$ fragment relative to the "$IrH_2$" moiety. When the temperature is lowered to 233 K, the spectrum becomes consistent with an $A_2BX_3$ spin system which can be interpreted by postulating that two of the phosphorus atoms of triphos, i.e., those in trans-position to a hydride ligand, differ from the third implying the presence of a static "(triphos)$IrH_2$" moiety and a rotating $\{AuPPh_3\}$ fragment. However, neither the room-temperature nor the low-temperature process is possible in the solid state and thus, in this phase, one would expect more than three phosphorus signals. Indeed, one observes six different resonances attributable to each of the six $^{31}$P-spins present in the molecule (see Figure 2, bottom trace). Given the relative positions of the non-hydrogen atoms in the solid-state structure, i.e., the presence of a $C_3$-symmetry axis and the near-eclipsed conformation of the $Au_3$ triangle relative to the triphos-$P_3$ plane, the observation of six resonances implies a static location of the hydride ligands, at least on the NMR time scale, and excludes that these two ligands are placed on the $C_3$ axis. It does not, however, provide information as to whether the bridging H-atoms are $\mu_2$ or $\mu_3$.

The $^{31}$P solid-state NMR spectrum of the rhodium dihydride complex is shown in Figure 2, upper trace. The interpretation of this spectrum is less simple as in this compound the difference in chemical shift between the triphos and $PPh_3$ ligands ($\Delta\delta$ = 7 ppm in solution) is considerably smaller than in the corresponding iridium complex ($\Delta\delta$ = 51 ppm in solution). Nevertheless, if in the case of the rhodium complex fast hydride site exchange of the type mentioned above were to occur, one would get a spectrum showing only two types of signals. However, as shown in Figure 2, the spectrum of the rhodium complex consists of more than the two resonances expected for a cluster having $C_3$ symmetry and, furthermore, the *three* resonances between 37 and 46 ppm can be readily assigned to three inequivalent phosphorus spins in the triphos ligand through their $^1J$(Rh,P) couplings.

In this context it is worth noting that the $^{31}$P solid-state NMR spectrum of $C_3$-symmetric [(triphos)$RuH_3\{AuPPh_3\}_3][PF_6]_2$, [**3**]-$[PF_6]_2$, does indeed show the presence of only two resonances, at 44.2 (triphos) and 40.4 ($PPh_3$) ppm, while that of the corresponding dihydride [(triphos)$RuH_2\{AuPPh_3\}_3][PF_6]$, [**7**]$[PF_6]$, which must have a lower symmetry, has an appearance similar to that of the corresponding rhodium complex.

In conclusion, we note that the solid-state $^{31}$P NMR spectra of [(triphos)$RhH_2\{AuPPh_3\}_3](CF_3SO_3)_2$, [**1**]$(CF_3SO_3)_2$, [(triphos)$IrH_2\{AuPPh_3\}_3](CF_3SO_3)_2$, [**2**]$(CF_3SO_3)_2$, and [(triphos)-$RhH_2\{AuPPh_3\}_3][PF_6]$, [**7**]$[PF_6]_2$, are best interpreted as resulting from molecules lacking any molecular symmetry. The 3-fold *crystallographic* symmetry is, therefore, best explained by assuming a *static disorder*.

### Mössbauer Spectroscopic Studies

The usefulness of $^{197}$Au Mössbauer spectroscopy for the classification and characterization of various gold compounds has been amply demonstrated[11] and extensively reviewed.[12] A large amount of data has been collected, mainly for gold(I) and gold(III) compounds with various coordination numbers and ligand types. Although much less information is available for gold clusters,[13] a Mössbauer study of **1** and of its congeners seemed

(11) (a) Faltens, M. O.; Shirley, D. A. *J. Chem. Phys.* **1970**, *53*, 4249. (b) Bartunik, H. D.; Potzel, W.; Mössbauer, R. L.; Kaindl, G. *Z. Phys. Phys.* **1970**, *240*, 1. (c) Parish, R. V. *Gold Bull.* **1982**, *15*, 51. (d) Parish, R. V. *Hyperfine Interact.* **1982**, *40*, 159. (e) Kongolo, K.; Bahr, A.; Friedl, J.; Wagner, F. E. *Met. Trans.* **1990**, *21B*, 239.

(12) (a) Parish, R. V. In *Mössbauer Spectroscopy Applied to Inorganic Chemistry*; Vol. 1, Long, G., Ed.; Plenum Press: New York, 1984; Vol. 1, p 577. (b) Williams, A. F. *Ibid.*, Vol. 2, p 429. (c) Parish, R. V. In *NMR, NQR, EPR and Mössbauer Spectroscopy in Inorganic Chemistry*; Burgess, J., Ed.; Ellis Horwood: Chichester, U.K., 1990; and references cited in these reviews.

(13) (a) van der Velden, J. W. A.; Bour, J. J.; Bosman, W. P. J.; Noordik, J. H. *J. Chem. Soc., Chem. Commun.* **1981**, 1218. (b) Bellon, P.; Manassero, M. N.; Sansoni, M. *J. Chem. Soc., Dalton Trans.* **1972**, 1481. (c) Manassero, M.; Naldini, L.; Sansoni, M. *J. Chem. Soc., Chem. Commun.* **1979**, 385. (d) van der Velden, J. W. A.; Bour, J. J.; Steggerda, J. J.; Beurskens, P. T.; Roseboom, M.; Noordik, J. H. *Inorg. Chem.* **1982**, *21*, 4321. (e) Schmid, G.; Pfeil, R.; Boese, R.; Bandermann, F.; Meyer, S.; Calis, G. H. M.; van der Velden, J. W. A. *Chem. Ber.* **1981**, *114*, 3634. (f) van der Velden, J. W. A.; Vollenbroek, F. A.; Bour, J. J.; Beurskens, P. T.; Smits, J. M. M.; Bosman, W. P. *Recl. Trav. Chim. Pays-Bas* **1981**, *100*, 148. (g) van der Velden, J. W. A.; Bour, J. J.; Bosman, W. P.; Noordik, J. H.; Beurskens, P. T. *Recl. Trav. Chim. Pay-Bas* **1984**, *103*, 13. (h) van der Velden, J. W. A.; Beurskens, P. T.; Bour, J. J.; Bosman, W. P.; Noordik, J. H.; Kolenbrander, M.; Buskes, J. A. K. M. *Inorg. Chem.* **1984**, *23*, 146. For further references see ref 12.

mandatory given the questions posed by the crystallographic results for the dihydrido-bridged cluster cations **1** and **2** and their conceivable hydride locations, structural predictions from our MO analysis (see later), and the solid-state $^{31}$P-NMR results described in the previous sections. The usual experimental conditions of a Mössbauer measurement obviously exclude any intra- or intermolecular exchange processes, and so a Mössbauer investigation, in principle, should provide a good chance to differentiate between a true 3-fold symmetry in the solid-state structure for **1** and **2**, as suggested by X-ray crystallography, and a less symmetric geometry coupled to a static disorder phenomenon, as revealed by the solid-state $^{31}$P-NMR data and indicated by MO calculations. Moreover, it seemed possible that Mössbauer data (isomer shifts, IS, quadrupole splittings, QS, peak intensities), e.g., for **1**, might even allow the assignment of $\mu_2$-edge-bridging or $\mu_3$-face-bridging situations for the hydride ligands. Thus, for a $\mu_2$ location, two of the gold atoms of **1** would be in contact with one hydrogen and one gold would be without direct Au–H bonding, while, for a $\mu_3$ position of the two hydrides, one gold atom would be connected to both of them and each of the two other gold centers would interact only with one hydride. Basically, there should be a correlation between the gold isomer shift values (IS) and the 6s occupation[14] of the gold atoms, which in turn should depend on the relative number of hydrogens interacting with them. The question is, of course, whether the differences in total *s*-electron density and/or the nonsymmetric charge distribution (the electric field gradient), which will determine the difference in IS and QS values, respectively, are large enough for different gold nuclei of hydrido clusters like **1** with either $\mu_2$- or $\mu_3$-hydrides to allow one to distinguish these possibilities or to at least exclude the presence of three equivalent gold atoms.

The EH calculations carried out for some Au clusters[15] seem to provide good correlations between Au 6p orbital occupations and quadrupole splittings, but these systems are not comparable to **1** and its congeners. To our knowledge, no gold compounds, which prima facie could serve as reasonable models for our hydrido clusters, have been studied by Mössbauer spectroscopy so far. As there are well-established, empirical linear correlations between QS and IS values for a large number of Au(I) as well as for Au(III) compounds,[16] a relative classification of **1** and its relatives in comparison to the data of known systems was also of some interest.

The Mössbauer spectra were measured for $[(triphos)RhH_2\{Au(PPh_3)\}_3](CF_3SO_3)_2$, **[1]**$(CF_3SO_3)_2$, as well as for the hexafluorophosphates $[(triphos)RhH_2\{Au(PPh_3)\}_3][PF_6]_2$, **[1]**$[PF_6]_2$, $[(triars)RhH_2\{Au(PPh_3)\}_3][PF_6]_2$, **[1′]**$[PF_6]_2$, and $[(triphos)IrH_2\{Au(PPh_3)\}_3][PF_6]_2$, **[2]**$[PF_6]_2$ (for details see the Experimental Section). Their IS and QS values and relative intensities for the best two-site fits are given in Table III. Figure 3 displays the spectrum obtained for **[2]**$[PF_6]_2$ chosen as a typical example as the $^{31}$P-NMR for **[2]**$(CF_3SO_3)$ was discussed in detail. Very similar spectra were obtained for all compounds, and their main features are discussed below.

There is *a distinct asymmetry of the measured doublet patterns*, with the right-hand component being broader. This could be due to the presence of two overlapping doublets, caused by two different gold sites with slightly different Mössbauer parameters. An alternative explanation would be a single-site situation, with unequal intensities for the components of the doublet arising from either a Goldanski–Karyagin effect[17] or from a slight orientational anisotropy of the crystallites of the sample in the Mössbauer experiment. The Goldanski–Karyagin explanation does not seem to be very probable, because it should be much less pronounced here than in, e.g., linear Au(I) compounds, and the sample anisotropy interpretation seems to be somewhat unlikely in view of the close similarity of all spectra. In fact the best least-squares fits for each cluster are obtained with a two-site model, expecially when the model uses two doublets for two types of gold atoms with different chemical shift values (viz. Table III), rather than two sites with similar chemical shift values and different quadrupole splittings. Thus, the absence of a symmetrical doublet in all cases is reasonably interpreted as excluding a structure with a static $C_3$ symmetry, i.e., with three equivalent gold atoms. We also note, that the two-site fit, as shown in the example of Figure 3, in all cases leads to one *weaker site*, presumably corresponding to one of the three gold atoms, which has also the *smaller isomer shift*, and a stronger site, corresponding to the two other equivalent Au centers. The relative intensities of the two doublets are not exactly 1:2, but the data were not fitted again with a ratio constrained to 1:2, as the approximate 1:2 ratio obtained was sufficiently close to be considered as conclusive.

The consistent correlation between the weaker doublet and the smaller IS is of particular interest, because it is in line with the usual assumption of a lower IS for lower total s-electron density and a lower occupation of the gold 6s orbital. Thus, the two-site model of Figure 3 and Table III means that the unique Au center in all our dihydro clusters is more electron deficient than the other two gold atoms. On the basis of the bonding model outlined later, the Mössbauer data would be consistent with a face-bridging situation, with two $\mu_3$-hydrides simultaneously interacting with a unique gold center, or an intermediate situation between $\mu_2$-

**Table III.** Mössbauer Parameters for Dihydro Cluster Dications $[(L)MH_2\{Au(EPh_3)\}_3]^{2+}$ (L = triphos, triars; M = Rh, Ir; E = P, As)

| cluster | IS[a] | QS[b] | W[c] |
|---|---|---|---|
| $[(triphos)RhH_2\{Au(PPh_3)\}_3](CF_3SO_3)_2$ | 3.58 | 7.42 | 1.91 |
| | 2.76 | 6.85 | 1.91 |
| $[(triphos)RhH_2\{Au(AsPh_3)\}_3][PF_6]_2$ | 2.98 | 6.79 | 1.82 |
| | 2.24 | 6.57 | 1.82 |
| $[(triars)RhH_2\{Au(PPh_3)\}_3][PF_6]_2$ | 3.15 | 7.50 | 1.79 |
| | 3.02 | 7.25 | 1.79 |
| $[(triphos)IrH_2\{Au(PPh_3)\}_3][PF_6]_2$ | 3.70 | 7.64 | 1.91 |
| | 3.06 | 7.06 | 1.91 |

[a] Isomer shifts ($mm\cdot s^{-1}$). [b] Quadrupole splittings ($mm\cdot s^{-1}$). [c] Line widths at half-maximum ($mm\cdot s^{-1}$). (Average standard deviations are less than $\pm 0.5$ $mm\cdot s^{-1}$).

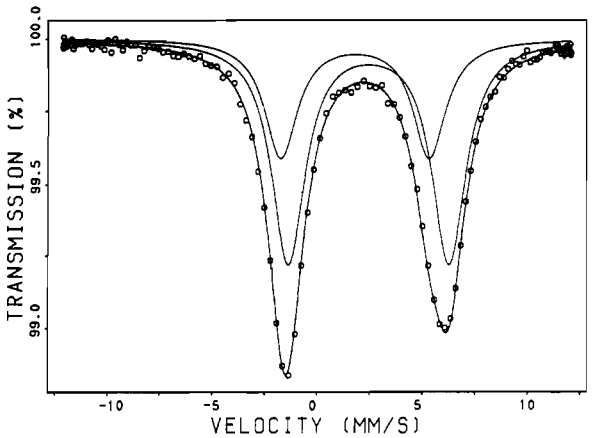


**Figure 3.** Mössbauer spectrum of $[(triphos)IrH_2Au(PPh_3)\}_3][PF_6]_2$, **[2]**$[PF_6]_2$. The IS scale is relative to the Pt metal source. Adding +1.23 $mm\cdot s^{-1}$ yields the data relative to metallic gold in Table III.

(14) Of course it is not only the 6s occupation but the total electron density at the Au nuclei, depending upon screening effects and other factors, which determines the isomer shifts. However, in a series of closely related molecules or ions, the 6s occupation trends should correlate with IS data.

(15) van der Velden, J. W. A.; Stadnik, Z. M. *Inorg. Chem.* **1984**, *23*, 2640 and references therein.

(16) Charlton, J. S.; Nicholls, D. I. *J. Chem. Soc. A* **1970**, 1484. See also refs 11 and 12.

(17) Greenwood, N. N.; Gibb, T. C. *Mössbauer Spectroscopy*; Chapman and Hall: London, 1971.

and $\mu_3$-bridging. The calculated net atomic charge for the singular Au center of our model cluster, i.e., $[(PH_3)_3Rh(AuPH_3)_3](\mu_3\text{-}H)_2^{2+}$ (see Figure 11, later) is +0.342, as compared to +0.236 for the two other symmetry-equivalent gold atoms. Accordingly the 6s AO occupations are 0.586 and 0.656 e$^-$, respectively. Apart from this qualitative correlation, we feel it would not be appropriate to further analyze our Mössbauer data on the basis of our EH–MO results, e.g., as done by van der Welden and Stadnik,[15] with respect to Au 6p occupation numbers and asymmetry factors as a measure for electric field gradients and QS data.

The second observation in our set of Mössbauer data concerns *the absolute magnitude of IS and QS values* for the series of dihydrido cluster dications. The values presented in Table III fall into the range found for peripheral (ligand coordinated) gold atoms in other Au clusters.[18] Moreover, if plotted into various IS–QS correlation diagrams in the literature,[12] the observed values of all four dihydrido systems of Table III fit perfectly into those for two-coordinate gold(I) complexes, and in particular they appear in the rather small range of data found for compounds of the type P–Au–X, being located at the lower end of the corresponding IS–QS scale. This is consistent with effectively linear (sp-hybridized) P–Au–X or As–Au–X (X = Rh, Ir) subunits in our clusters and with an overall +I oxidation state of the gold atoms. In agreement with the data for $[AuCl(Ph_3P)]$ and $[AuCl(Ph_3As)]$[19] (IS 4.08 and 3.08, respectively), the isomer shifts for $[(triphos)RhH_2\{Au(PPh_3)\}_3]^{2+}$ (3.58, 2.76) are larger than those of the As derivative $[(triphos)RhH_2\{Au(AsPh_3)\}_3]^{2+}$ (2.98, 2.24) and follow the order of ligand donor capacity $AsPh_3 > PPh_3$. When compared with the series $[AuX(PPh_3)]$ (X = CN, Cl, I; IS = 5.07, 4.08, 4.03; QS = 10.25, 7.43, 7.36, respectively), the $RhP_3$ and $IrP_3$ caps of our clusters seem to be less "soft" and overall weaker donor groups than halogens X in P–Au–X compounds, with less direct 6s bonding to gold. This conclusion seems reasonable, as the capping metal unit interacts with three AuL fragments simultaneously, although the bridging hydrogens will also play a role here, and their exact influence is difficult to assess. If, as above, one assigns the smaller IS values (the weaker site, the unique Au) to the gold atom in contact with two bridging hydrogens, then the higher IS values of the two other Au centers would indicate more direct covalency to Rh and Ir for the latter Au atoms, as expected.

Overall, the Mössbauer data for our series of dihydrido clusters exclude pure $\mu_2$-structures and are most consistently interpreted on the basis of the structure with two $\mu_3$- or quasi-$\mu_3$-hydrogens, as suggested by MO theory and are compatible with the solid-state NMR results.

### Vibrational Studies

Infrared[20] and incoherent inelastic neutron spectroscopy (IINS) studies[21] were undertaken in order to obtain a more precise description of the positions of the hydride ligands on the $MH_xAu_3$ clusters (M = Ru, $x = 3$; M = Rh, $x = 2$). The main characteristic feature of the infrared spectrum of $[1](CF_3SO_3)_2$, in the region 2000–1400 cm$^{-1}$, is the presence of three weak bands at 1962, 1891, and 1812 cm$^{-1}$. These are followed by a very broad quite asymmetric band with maximum at 1606 cm$^{-1}$: on the high-energy side of this feature there appears to be an absorption with a maximum at ca. 1671 cm$^{-1}$. The only significant difference between this spectrum and that of the corresponding deuteride $[(triphos)RhD_2\{Au(PPh_3)\}_3](CF_3SO_3)_2$, in the same region, is the shape and the intensity of the broad feature with maximum at 1605 cm$^{-1}$: both the overall intensity of this band and the asymmetry on the high-energy side have decreased. The difference between the two spectra indicates the presence of a broad band centered at ca. 1650 cm$^{-1}$. Thus, one can postulate that, in this region, one of the modes associated with the "$RhH_2Au_3$" species is at ca. 1650 cm$^{-1}$, a range which is typical for bridging hydrides in general and of edge ($\mu_2$) bridging in particular.[22] The higher frequency bands mentioned above are due to the organic ligands triphos and $PPh_3$. These occur at ca. 1971, 1890, 1815, and 1737 cm$^{-1}$ in $[RhCl_3(triphos)]$. Similarly placed bands are also observed in $[AuCl(PPh_3)]$.

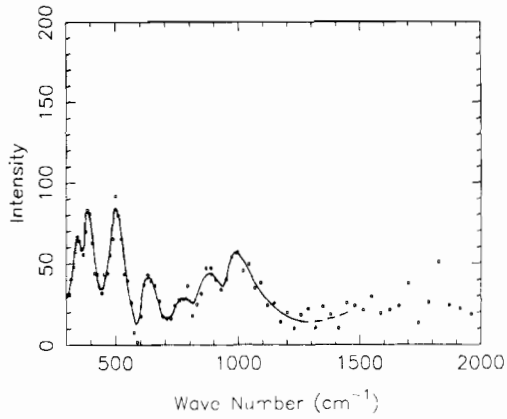


**Figure 4.** IINS spectrum of $[(triphos)RhH_2\{Au(PPh_3)\}_3](CF_3SO_3)_2$, $[1](CF_3SO_3)_2$. (The full line is meant only as a visual aid.)

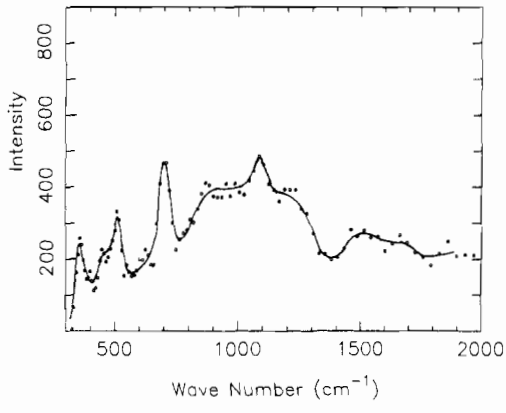


**Figure 5.** IINS spectrum of $[(triphos)RuH_3\{Au(PPh_3)\}_3][PF_6]_2$, $[3][PF_6]_2$. (The full line is meant only as a visual aid.)

A comparison of the spectra of $[(triphos)RuH_3\{Au(PPh_3)\}_3][PF_6]_2$, $[3][PF_6]_2$, with those of the corresponding dideuteride shows, once again, that the broad feature with a maximum at 1605 cm$^{-1}$ is the superimposition of unidentified ligand modes with $RuHAu_x$ stretching bands.

In order to clarify the assignments of the infrared spectra, IINS spectra of compounds $[1](CF_3SO_3)_2$ and $[3][PF_6]_2$ were recorded as this method reveals only modes involving hydrogen atoms (see Experimental Section). The spectra of these compounds obtained by this technique are shown in Figures 4 and 5, respectively, and the data and relative assignments are collected in Table IV. For comparison purposes similar data for related compounds are summarized in Table V.[23]

The interpretation of these spectra is best done by starting from a model involving $\mu_2$-bridging hydrides as the presence of bands above 1400 cm$^{-1}$ in the vibrational spectra excludes a pure $\mu_3$-model.

The normal modes of vibration of a $\mu_2$-hydride ligand may be

(18) See ref 12a, p 603.
(19) Reference 12a, Table 2, p 583.
(20) Kaesz, H. D.; Saillant, B. R. *Chem. Rev.* **1972**, *72*, 231.
(21) Lechner, R. E.; Riekel, C. In *Neutron Scattering and Muon Spin Rotation*; Springer Tracts in Modern Physics; Springer Verlag: Berlin, 1983; Vol. 101, p 3.
(22) (a) Cooper, C. B.; Shriver, D. F.; Onaka, S. In *Transition Metal Hydrides*; Bau, R., Ed.; Advances in Chemistry Series No. 167; American Chemical Society: Washington, DC, 1978; p 232. (b) Roziere, J.; Potier, A. *Bull. Chem. Soc. Fr.* **1982**, I-339.
(23) Graham, D. Ph.D. Thesis, University of Durham, Durham, U.K., 1980.

**Table IV.** IINS Data for the Cationic Complexes $[(triphos)RhH_2\{Au(PPh_3)\}_3]^{2+}$, **1**, and $[(triphos)RuH_3\{Au(PPh_3)\}_3]^{2+}$, **3**

| | M = Rh (**1**) | M = Ru (**3**) |
|---|---|---|
| $\nu_{as}$(M–H–M) | *a* | 1650[a] (m, br) |
| combination or overtone | 1300[b] (w) | 1200[c] (sb) |
| $\nu_s$(M–H–M) | 1010 (s) | 1080 (vs) |
| combination | 870[d] (s) | 880[f] (mb) |
| | 760[f] | |
| δ(M–P–C) | 640 (m) | 380 (vs) |
| δ(in-plane M–H–M) | 510 (vs) | 710 (vs) |
| δ(out-of-plane) | 395 (vs) | 490 (s) |
| | 350 (vs) | |

[a] See discussion. [b] Overtone 640 × 2 = 1280. [c] 710 + 490 = 1200. [d] 510 + 350 = 860. [e] 490 + 380 = 870. [f] 395 + 350 = 745 or overtone 395 × 2 = 790.

described[24] in terms of two stretching modes, i.e., a symmetric and an antisymmetric metal–hydrogen stretch, and two deformation modes of the M–H–M framework. Previous studies have shown that the stretching modes occur in the range 800–1800 $cm^{-1}$, whereas the deformation modes fall into the range 300–800 $cm^{-1}$. IINS intensities are primarily governed by the amplitudes of the motion of the hydrogen atoms involved in the particular mode.[25] Thus, the high-frequency $\nu_{as}$(MH) will have a low intensity, whereas the deformation modes would have higher IINS intensities.

The IINS spectrum of the ruthenium cation **3** will be discussed first. As the IINS spectra of $\mu_2$-H compounds are frequently more complex than the above description of the hydride vibrations would suggest, the proposed assignments are based on our structural data obtained by X-ray diffraction and on the assumption of the quasi-$\mu_3$-coordination discussed earlier. By analogy with the results from several other examples of such compounds (see Table V), we assign the peak at 1080 $cm^{-1}$ to $\nu_s$(RuH). Furthermore, if one takes into account the broad IR band at ca. 1650 $cm^{-1}$ and the shape of the IINS band in this region, one could make the following additional assignments: the broad absorption centered at ca. 1550 $cm^{-1}$ consists of two overlapping bands, one at ca. 1650 $cm^{-1}$ and the other at ca. 1500 $cm^{-1}$. The former could be due to $\nu_{as}$, and the latter could be a combination band of $\nu_s$(M–H–M) = 1010 $cm^{-1}$ (s) and δ(out-of-plane) = 396 $cm^{-1}$ (vs). The bands at 380 and 700 $cm^{-1}$ are then assigned to the out-of-plane and in-plane deformations, respectively, again in accordance with many previous studies. The remaining well-defined band at 490 $cm^{-1}$ may be attributed to skeletal motion that involves the hydride moving along with it. The broad shoulders around $\nu_s$(RuH) may be assigned to overtone and combination bands which do have significant intensity in the IINS. However, if one assumes that the very broad feature centered at 1550 $cm^{-1}$ is a single band, this must be assigned to $\nu_{as}$(RuH). In this case the difference in frequency between the IINS and IR values may be due to the lower resolution of the neutron experiment in the high-energy region combined with the use of the "difference" technique (see Experimental Section).

The data for the rhodium cation **1** are of somewhat poorer quality and, therefore, less conclusive. Nonetheless, we can attempt an assignment by analogy with the ruthenium compound. The broad peak at 1010 $cm^{-1}$ and the peaks at 370 and 510 $cm^{-1}$ are, therefore, assigned to $\nu_s$(RhH) and the two deformation modes, respectively, while the remaining features may be combinations, overtones, or skeletal modes. The poor statistics in the region above 1500 $cm^{-1}$ do not allow a reliable identification of $\nu_{as}$(Rh–H).

(24) Braid, I. J.; Howard, J.; Tomkinson, J. *J. Chem. Soc., Faraday Trans.* **1983**, *2*, *79*, 253.
(25) Howard, J.; Waddington, T. C. Molecular Spectroscopy with Neutrons. In *Advances in Infrared and Raman Spectroscopy*; Clark, R. J. H., Hester, R. E., Eds.; Wiley: Chichester, U.K., 1980; Vol. 7, p 86.

In conclusion, the IR and IINS data, taken together, are consistent with the proposed quasi $\mu_3$-model for the bonding of the bridging hydride ligands.

## Bonding and Electronic Structure: MO Model Calculations

As mentioned earlier, the available spectroscopic and—in particular—structural information for the two novel cluster cations **1** and **3**, together with those for their congeners **5** and **6**, provides a highly interesting set of complementary and mutually related data. It is obvious that there must be a common pattern of electronic structures and a closely related bonding picture for **1**, **3**, **5**, and **6** as all four systems have the same valence electron count, despite (1) their different capping $ML_3$ units, (2) their different numbers of cluster hydrogens, and (3) their respective +1 or +2 charge. As mentioned earlier, the dihydrido–ruthenium cluster $[(triphos)RuH_2\{Au(PPh_3)\}_3]^+$, **7**, has also been obtained. However, up to now it has not proved possible to unambiguously determine its X-ray crystal structure.

The purpose of this section is to derive a general bonding scheme based upon MO theory and appropriate model calculations. We want to address questions related mainly to systems **1** and **3**, trying to analyze their similarities and differences. As it was not possible to locate the hydrogen positions in **1**, and because it is clear that the hydrogen ligands in these gold clusters play a major role in determining their structures and stabilities, we will particularly try to understand their preferred locations and their influence upon the overall bonding situation and the molecular geometries.

Given the above-mentioned experimental findings of facile dynamic processes for **1**, **3**, and their analogs, it is clear that we are dealing with very soft potential energy surfaces and very shallow, multiply degenerate energy minima. Such a situation may cause severe problems if we want (1) to reliably derive minimum structures from MO calculations, especially when we are dealing with heavy metal systems within the framework of the extended Hückel approach, and (2) to calculate hydride positions by geometry variation and optimization. Fortunately, however, we can use the experimental structure of **3** as an independent check. As mentioned earlier, a very similar structural arrangement is found for the $ReAu_3H_3$ core of **5**.[26] It seems, therefore, reasonable to begin our analysis with the trihydride systems, in order to check if our model calculations yield results reasonably in agreement with the structural findings for **3** and **5**. Furthermore, the higher symmetry of the trihydrides should facilitate an MO description.

For obvious reasons we shall use simplified models for **1**, **3**, **5**, and **6**, i.e., the cluster frame, displayed in **8**, in which the triphos

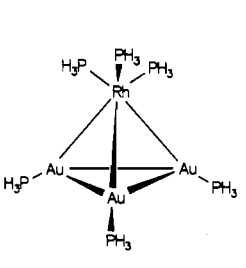


*8*

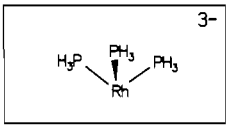


*9*

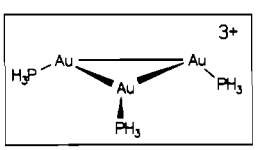


*10*

as well as the triphenylphosphine ligands are replaced by $PH_3$. The hydrides are not included in **8** as yet, because conceptually and quite formally we may view clusters **1**, **3**, **5**, and **6** as triply, doubly, or singly protonated, isoelectronic $P_3Rh(AuP)_3$, $P_3Ru$-

**Table V.** Selected IINS Data (in $cm^{-1}$) for Hydrido-Bridged Complexes

| | $\nu_{as}$ | $\nu_s$ | δ(in plane) | δ(out of plane) | ref |
|---|---|---|---|---|---|
| $[Re_3H_3(CO)_{12}]$ | 1675 (m) | 1159 (sb) | 531 (vs) | 324 (bs) | 23 |
| $[Mn_3H_3(CO)_{12}]$ | 1661 (s) | 983 (m) | 606 (vs) | 336 (vs) | 23 |
| $[Os_3H_2(CO)_{12}]$ | 1483 (s) | 1225 (s) | 730, 672 (vs) | 430 (vs) | 23 |
| $[Ru_4H_4(CO)_{12}]$ | 1600 (m) | 1294 (s) | 623 (vs) | 359 (vs) | 23 |
| $[FeRu_3H_2(CO)_{13}]$ | 1471 (msh) | 1322 (vs) | 646 (vs) | 362 (s) | 23 |
| $[(triphos)RhH_2\{Au(PPh_3)\}_3]^{2+}$ | *a* | 1010 (s) | 510 (vs) | 395, 350 (vs) | *b* |
| $[(triphos)RuH_3\{Au(PPh_3)\}_3]^{2+}$ | *a* | 1080 (vs) | 710 (vs) | 490 (s) | *b* |

[a] See discussion. [b] See Table IV.

$(AuP)_3^-$, $P_3Re(AuP)_3^{2-}$, and $P_2(CO)Rh(AuP)_3$ tetrametallic anionic or neutral cores.

This approach has been employed before in electronic structure descriptions of hydrido cluster compounds[27] and allows us to start out from the bonding picture of **8**, adding the protons necessary to build up the models for **1**, **3**, **5**, and **6** in a second step. We will, furthermore, restrict all model calculations to Rh in the capping $ML_3$ unit and to a common core geometry for **8** and its protonated derivatives, with fixed Rh–Au and Au–Au distances, thus comparing $[(PH_3)_3Rh(AuPH_3)_3](H)_3^{3+}$ as a model for **3** and **5** with $[(PH_3)_3Rh(AuPH_3)_3](H)_2^{2+}$ as a model for **1** and with $[(PH_3)_3Rh(AuPH_3)_3](H)^+$ resembling **6**. This approach within the EH–MO model allows a direct comparison of charges, overlap populations, etc. and of their trends in the computations, e.g. as a function of the number of cluster hydrogens or of geometries.

It is most convenient then to start out from the neutral metallotetrahedrane fragment **8** itself and to regard this building block as being composed of two even simpler fragments: a pyramidal "conical" $Rh(PH_3)_3^{3-}$ unit and a triangular $[Au(PH_3)]_3^{3+}$ moiety (both $C_{3v}$ symmetry), shown in **9** and **10**, respectively. The fragment charges, of course, are arbitrary and could have been chosen in a different way, e.g., taking both the Rh fragment and the $Au_3$ fragment as neutral entities, but we prefer the simple isolobal analogy of a single $Au(PH_3)^+$ fragment to a proton,[3] if we take **9** and **10** as our starting points. It is well established, that $d^{10}$-$AuL^+$ units at a first approximation essentially only contribute a single valence orbital, a low-lying sp-hybrid MO (mainly s-character with small p- and d-contributions, empty for $AuL^+$, $AuPH_3^+$, etc.) to cluster bonding, because the gold p-AOs are to high in energy and the gold d-shell is contracted and part of the inactive atomic core (relativistic effects seem to play a role here).[28]

The valence orbitals of a pyramidal $ML_3$ fragment, $1a_1$, 1e, 2e, and $2a_1$, have been repeatedly described in detail in the literature[29] and need not be reiterated here. They are shown on the left side of Figure 6, which represents an interaction diagram between fragments **9** and **10** for the $C_{3v}$ cluster **8**. The mutually eclipsed orientation has been chosen because this is close to the relative orientation found in the available di- and trihydride structures of **1**, **3**, and **5**.

Orbitals 1e and $1a_1$ of **9** (mainly $x^2-y^2$, $xy$, and $z^2$, d-type lone pairs at Rh) are the remnants of the $t_{2g}$ set of an octahedral

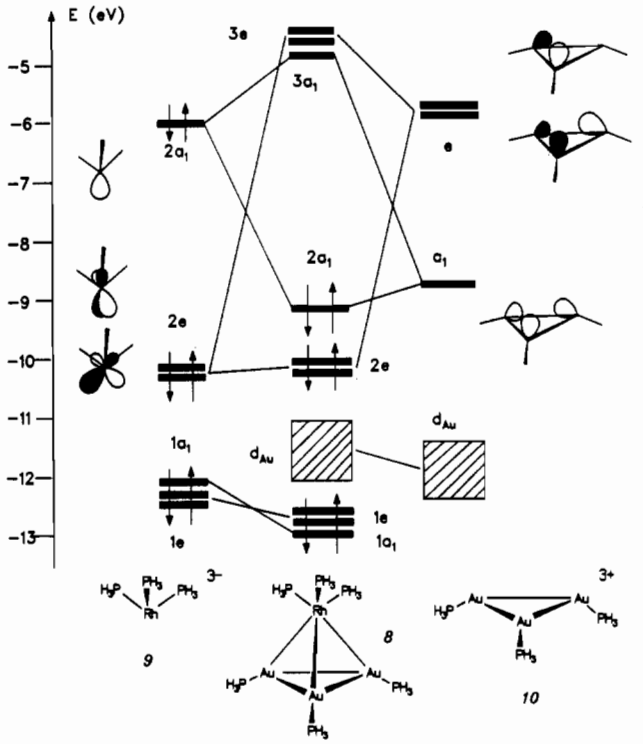


**Figure 6.** Interaction diagram between a $C_{3v}$ $d^{10}$ fragment $(PH_3)_3Rh^{3-}$, **9**, and the $C_{3v}$ trimeric gold phosphine unit $(AuPH_3)_3^{3+}$, **10**, yielding the valence MOs of the neutral cluster unit $(PH_3)_3Rh(AuPH_3)_3$, **8**.

complex while the familiar levels 2e and $2a_1$ (mainly *xz*, *yz*, somewhat rehybridized, and an sp hybrid with some d-admixture, filled for the triply negative fragment $Rh(PH_3)_3^{3-}$) are predominantly responsible for the interaction with the $[Au(PH_3)]_3^{3+}$ trimetallic unit. The relevant orbitals of the latter (also with $C_{3v}$ symmetry, the $PH_3$ ligands on gold bent down as in **8**) are given on the right side of Figure 6 and are easily derived as appropriate linear combinations of the MOs of a single $Au(PH_3)^+$ fragment. Above a nest of 15 d-type levels (3 × the 5d-AOs of the gold centers), close in energy to the 1e and $1a_1$ MOs of $Rh(PH_3)_3^{3-}$, appears the in-phase combination $a_1$ of the three gold sp-hybrids. The two corresponding members of the related e set of $[Au(PH_3)]_3^{3+}$ are found at much higher energy, and (not shown in the diagram) the linear combinations of the gold p-orbitals are at still higher energy.

The large energy gap between $a_1$ and e of **10** is already indicative of an appreciable overlap between the three sp-hybrids of the three $Au(PH_3)^+$ subunits at the given Au–Au distance, which, in turn, must lead to significant Au–Au bonding within the $Au_3$ triangle if the $a_1$ linear combination of the $[Au(PH_3)]_3^{3+}$ fragment **10** receives electron density. This is exactly what happens in the composed cluster model **8**, because the dominant interaction between the two subunits of Figure 6 involves $2a_1$ of **9** and $a_1$ of **10**, which overlap strongly due to their matching symmetry and spatial extension (group overlap integral $\langle 2a_1/a_1 \rangle = 0.593$). A Rh–Au as well as Au–Au bonding, totally symmetric cluster MO

(26) The structural plot of cation **5**, in ref 9, represented in a recent review article (Mueting, A. M.; Bos, W.; Alexander, B. D.; Boyle, P. D.; Casalnuovo, J. A.; Balaban, S.; Ito, L. N.; Johnson, S. M.; Pignolet, L. H. *New. J. Chem.* **1988**, *12*, 505) nicely illustrates its molecular geometry including the assumed hydride locations. In **3**, given the experimental error, and the uncertainty of H positions in X-ray structures, the Au–H distances to both Au atoms of a $RuAu_2$ face would not be significantly different.

(27) Hoffmann, R.; Schilling, B. E. R.; Bau, R.; Kaesz, H. D.; Mingos, D. M. P. *J. Am. Chem. Soc.* **1978**, *100*, 6088.

(28) (a) Pyykkö, P. *Chem. Rev.* **1988**, *88*, 563. (b) Pitzer, K. S. *Acc. Chem. Res.* **1979**, *12*, 271. (c) Pyykkö, P.; Desclaux, J. P. *Acc. Chem. Res.* **1979**, *12*, 276. (d) Scherbaum, F.; Grohmann, A.; Müller, G.; Schmidbaur, H. *Angew. Chem.* **1989**, *101*, 464; *Angew. Chem., Int. Ed. Engl.* **1989**, *28*, 463. (e) Rösch, N.; Görling, A.; Ellis, D. E.; Schmidbaur, H. *Angew. Chem.* **1989**, *101*, 1410; *Angew. Chem., Int. Ed. Engl.* **1989**, *28*, 1544.

(29) Albright, T. A.; Burdett, J. K.; Whangbo, M. H. *Orbital Interactions in Chemistry*; Wiley: New York, 1985; and references therein.

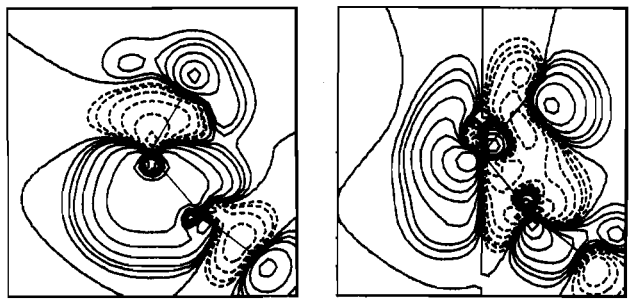

11 ($2a_1$) 13 ($2e_s$)

**Figure 7.** Contour plots of the highest occupied MOs of **8**, $2a_1$ and 2e. (Only the $2e_s$ component is shown.) The plots are in a plane that contains the capping Rh atom, one of its $PH_3$ P-centers, one gold atom, and the $PH_3$ ligand P-center of the latter, i.e., in a plane of symmetry of the $C_{3v}$ cluster fragment **8**. Solid (broken) lines represent positive (negative) values of the corresponding wave functions. Zero contour lines are also shown.

$2a_1$ emerges for **8** and is the HOMO. Its antibonding counterpart ($3a_1$, empty) is separated from the $2a_1$ HOMO by a large energy gap.

A second relevant interaction occurs between 2e of **9** and e of **10**, leading to the occupied cluster level 2e below the HOMO, which is mainly Rh–Au bonding. Its antibonding analog 3e lies above the cluster LUMO $3a_1$. The bonding linear combination 2e for the composite system **8** does not appear to be stabilized compared to the 2e MOs of $Rh(PH_3)_3^{3-}$, from which it originates. This is simply due to some destabilizing interactions mainly with the lower lying d-block levels 1e of $Rh(PH_3)_3^{3-}$, which keep the resulting 2e of **8** from going down and which, in turn, are themselves lowered in energy. These carry part of the overall stabilization and lie somewhat below the 15 gold-centered d-block MOs of **8**. The interaction between 2e of **9** and e of **10**, due to their smaller overlap ($\langle 2e/e \rangle = 0.2717$) and their larger energy separation, is much less pronounced than that between the two fragment levels of $a_1$ symmetry. In **8** the formerly empty MO $a_1$ of the $[Au(PH_3)]_3^{3+}$ fragment becomes occupied by 1.441 electrons. In addition a total of 0.5012 electrons is transferred to its e orbital set. The resulting metal–metal overlap populations of the cluster model **8** accordingly are quite high: 0.3616 for the three Rh–Au bonds and 0.1500 for the three Au–Au bonds. Practically all of this bonding character can be traced back to the three top cluster levels 2e and $2a_1$ of Figure 6 and their 6 electrons. Schematic representations of these $2a_1$ and 2e wave functions are shown in **11–13**.

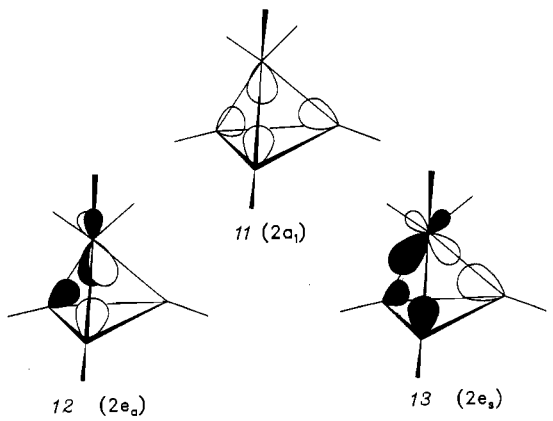

11 ($2a_1$)

12 ($2e_a$) 13 ($2e_s$)

Contour diagrams for $2a_1$ (**11**) and the symmetric 2e-set component $2e_s$ (**13**), plotted in one of the planes of symmetry of **8** (containing one of the Rh–Au vectors), are displayed in Figure 7.

The HOMO $2a_1$ of **8** is localized to one-third at the $Rh(PH_3)_3$ subunit, while the 2e orbital below the HOMO carries 75% $Rh(PH_3)_3$ contribution. The charge distribution on the metal centers of **8** reveals a large –2.02 negative charge at the Rh center and a practically uncharged set of Au atoms (Mulliken charges –0.06). This high charge separation indicates, qualitatively, that a cluster molecule of type **8**, without any $H^+$ added, should be kinetically unstable and highly reactive, although it may be a bound and thermodynamically stable species, e.g. in the gas phase.

The computed charges and overlap populations for **8** in the eclipsed (**14a**) and the staggered (**14b**) geometry will have to be compared with the "protonated", hydrogen-containing derivatives later.

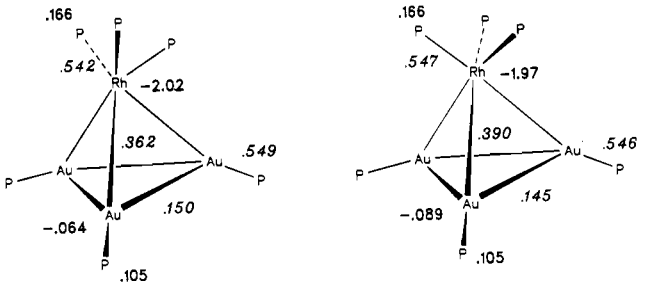


14a 14b

Obviously our restriction to keep **8** in an eclipsed rotational orientation of the $P_3Rh$ toward the $(AuP)_3$ moiety, adapted to the observed structures of **1**, **3**, and **5**, does not necessarily have to be the energetically best choice, as it puts the Rh atom into a quasi trigonal prismatic environment. $(PH_3)_3Rh(AuPH_3)_3$ might be expected on qualitative grounds to prefer a staggered conformation, reconstituting an octahedral ligand arrangement at the capping site. This is indeed the case, and our calculations show **8** to possess a barrier of 6 kcal for $(PH_3)_3Rh$ versus $(AuPH_3)_3$ rotation, with the staggered structure at lowest energy.

The analysis of this slight preference is straightforward and closely related to that presented for $ML_3$–polyene organometallic systems in the literature.[30] It is essentially based upon the appearance of the $(PH_3)_3Rh$ fragment's 1e and 2e orbitals, i.e. their "tilt", which leads to a better overlap of 2e of the rhodium fragment **9** with e of $(AuPH_3)_3^{3+}$ in the staggered, octahedral geometry and to less repulsion of 1e of **9** with occupied gold d-levels.

Compared to Figure 6, the 2e levels of staggered $(PH_3)_3Rh(AuPH_3)_3$ are slightly stabilized, and **14b** reveals a concomitant slight strengthening of the Rh–Au bonds, a very small decrease in Au–Au bonding, and a slightly larger charge transfer from the Rh to the $Au_3$ sites. Of course a barrier of only 6 kcal means essentially free rotation of the $(PH_3)_3Rh$ fragment (or, alternatively, the $(AuPH_3)_3$ triangle) in **8**, as expected for two 3-fold rotors loosely bound to each other through multicenter bonding.

It is relevant to note that for the less stable eclipsed structure of **8** the electron density of the Rh–Au bonding frontier MOs **11** and **12** has its maximum extension in and above the cluster faces, as nicely visible in the plots of Figure 7, where the big lobes on the left side of each wave function penetrate the $RhAu_2$ faces. This is a simple corollary of viewing the $(PH_3)_3Rh^{3-}$ cap as an octahedral complex with three lone pairs occupying three equivalent localized hybrid orbitals pointing toward the corners of the octahedron. This feature will of course influence and determine the location of hydrogen atoms, when we shall discuss the structures of the various protonated forms of $(PH_3)_3Rh(AuPH_3)_3$, which are to mimic the actual hydride clusters. The protons should go for the positions of best overlap with the frontier

(30) Albright, T. A.; Hofmann, P.; Hoffmann, R. *J. Am. Chem. Soc.* **1977**, *99*, 7546.

orbitals of $(PH_3)_3Rh(AuPH_3)_3$, where they can get the strongest interaction and the largest charge transfer to their empty 1s AOs.

On the basis of our analysis of **8**, we now may turn to these "protonated" derivatives, the models for **1**, **3**, **5**, and **6**, and we will begin with the trihydride $[(PH_3)Rh(AuPH_3)_3](H)_3^{3+}$, representing a model for the Ru cation **3**.

There are several limiting, idealized, and symmetric structures possible for this trihydrogen cluster, differing in (i) their H-atom positions and (ii) their rotational orientation of the $(PH_3)_3Rh$ fragment vis-a-vis the $(AuPH_3)_3$ triangle. Schematic representations ("top views") are depicted in **15–17** to indicate staggered (**15**, **16**) or eclipsed (**17**, **18**) structures and $\mu_2$-Rh–Au edge-bridging (**15**, **17**) or $\mu_3$-$RhAu_2$ face-bridging (**16**, **18**) hydrogen locations.

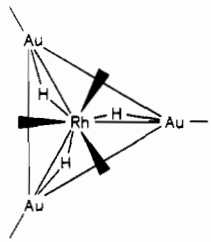


*15*

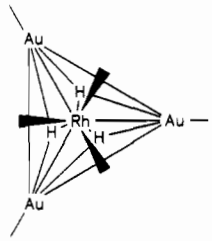


*16*

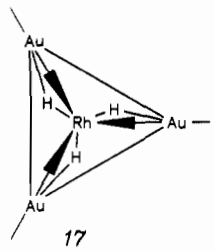


*17*

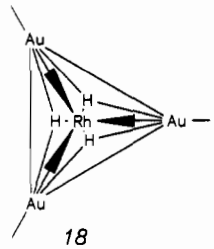


*18*

Starting out from **15** (staggered, $\mu_2$), we can reach **16–18** by varying only two geometric parameters, if we keep the Rh–H and the Au–H distances fixed. These two variables are shown in **19**,

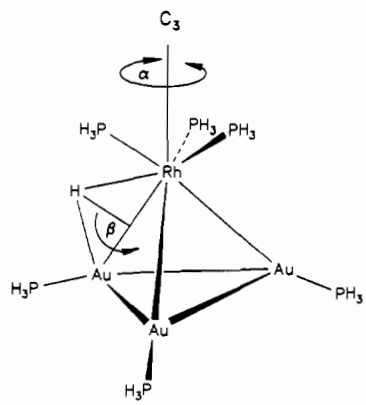


*19*

namely the rotational angle $\alpha$ of the $(PH_3)_3Rh$ unit with respect to the $C_3$ axis of the cluster and the angle $\beta$, which is the dihedral angle between the $C_3$ axis and the vectors pointing from the midpoints of the Rh–Au edges to the $\mu_2$-hydrogen atoms (shown for just one H in **19** for simplicity).

Varying $\beta$ from 0° (pure $\mu_2$-H positions) to smaller values allows the hydrogen centers to "lean over" toward a face-bridging $\mu_3$-position, as observed for the real molecules **3** and **5**. If both $\alpha$ and $\beta$ are varied independently, the idealized structures **15–18** and all waypoints in between can be covered.

Accordingly, $E = E(\alpha,\beta)$ was computed for $[(PH_3)_3Rh(AuPH_3)_3](H)_3^{3+}$, starting from **15** and varying $\beta$ from 0° ($\mu_2$) to 110°, independently rotating the $(PH_3)_3Rh$ tripod by 60° in

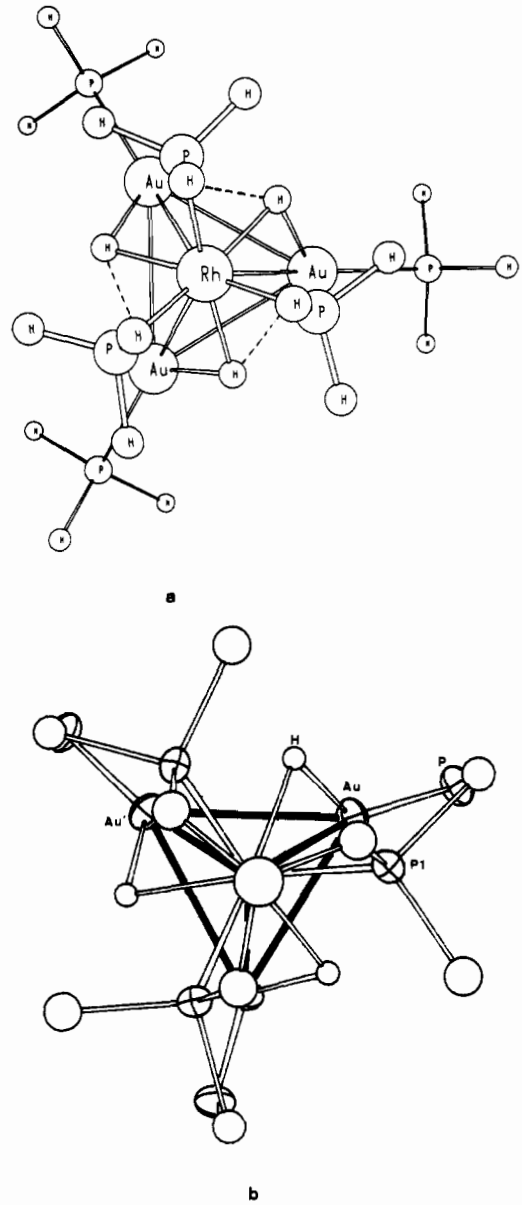


**Figure 8.** Views of the (a) optimized geometry of the model trihydride cation $[(PH_3)_3Rh(AuPH_3)_3](H)_3^{3+}$ and (b) an ORTEP plot of $[(triphos)Ru(AuPPh_3)_3](H)_3^{2+}$ dication (**3**).

both possible directions, con- or disrotatory with the hydrogen motions. In all geometry variations the Rh–H and Au–H distances within the moving Rh–H–Au triangles were kept fixed at 1.8 Å, which is reasonably close to the (rather approximate) X-ray values for **2** (Rh–H = 1.9(2) Å, Au–H = 1.7(2) Å).[31]

In Figure 8 the resulting minimum structure (a), close to **18**, is compared to an ORTEP plot (b) of the $P_3Ru(AuP)_3(H)_3$ core of the real system **3**. The agreement is surprisingly good. As found for **3**, the capping unit of our model system prefers a nearly eclipsed orientation (10° off), and the three hydrides are in a position, which is close to $\mu_3$, with $\beta = 80°$ and with Au–H distances to the opposite gold atoms on each face of 2.0 Å.[22] Moreover, the relative rotameric positions of the $(PH_3)_3Rh$ cap and the bridging hydrogens are precisely as in **3**.

The hydrides occupy positions exactly trans to the phosphines of the Rh fragment, thus forming a $(PH_3)_3Rh(H)_3$ octahedron,

(31) The same calculations were performed for Rh–H and Au–H = 165 pm, to check qualitatively the influence of variable M–H distances, which cannot be optimized reliably in EH. The qualitative conclusions remain unchanged.

(32) For $\beta = 90°$ this Au–H distance becomes 1.80 Å, placing the H atoms into an equidistant $\mu_3$-bonding situation.

which caps the $(AuPH_3)_3$ triangle with its $(H)_3$ face, just as described in the work on the Re trihydride **5**.[9,26]

So far our model calculations with their geometric restrictions seem to mimic well the experimental structure in the trihydrogen system. We note that the potential energy surface $E = E(\alpha,\beta)$ for $[(PH_3)_3Rh(AuPH_3)_3](H)_3^{3+}$ in the vicinity of its minimum structure (Figure 8) is very soft. Moving the hydrogens away from $\mu_3$ toward $\mu_2$ until a 2.6 Å distance from the opposite gold atoms is reached, and rotating the $(PH_3)_3Rh$ fragment by as much as 20–30° in ether sense, only raises the total energy by less than 10 kcal.

Further deviations toward structures **15**, **16**, or **17** are increasingly destabilizing, however. For all different rotational orientations of the $(PH_3)_3Rh$ cap the three hydrogens prefer a face-bridging position and the most unfavorable structure is **17** with $\mu_2$-H atoms and an eclipsed cluster skeleton.

At this point one must remember the facile dynamic processes observable already at low temperature for **1** or **3** in solution by NMR spectroscopy. Their interpretation, involving the relative rotation of an $(AuP)_3$ triangle relative to an intact $P_3RhH_3$ fragment, seems to imply (assuming the latter to remain octahedral) that geometries like **15** (staggered, $\mu_2$) have to be passed along the $(AuP)_3$ rotation itinerary.

Our model calculations put **15** much too high in energy to be accessible as an intermediate. This may be partly caused by our constraint to fix both Rh–H and Au–H distances at 1.8 Å, but given the inherent limitations of the EH model for optimizing bond lengths, we did not make any attempts to compute detailed reaction pathways for an $(AuP)_3$ rotation or for hydrogen ligand scrambling. Thus, we restrict the discussion to the static minimum structures obtained via restricted geometry optimizations as described above.

If we perform the same type of optimization for $[(PH_3)_3Rh(AuPH_3)_3](H)_2^{2+}$ and for $[(PH_3)_3Rh(AuPH_3)_3](H)^+$, our simplified models for **1** and for a monohydride like **6**, the minimum energy locations for the hydrogens in the dihydride case are again in the close vicinity of a $\mu_3$-bonding mode. As in the case of the trihydride model, an extremely soft energy minimum is found for a nearly eclipsed $(PH_3)_3Rh$ orientation (again 10° off), when we compute $E = E(\alpha,\beta)$ in a conrotatory and disrotatory fashion.

As the trihydride model is in good agreement with experiment, we feel quite confident that the minimum structure for the dihydride, as depicted in Figure 9a, also represents the correct picture of the preferred hydrogen positions in the static structure of **1**, where the H ligands could not be refined.

At this point we parenthetically mention that there exists a beautiful analogy of **1** and the computed molecular geometry of $[(PH_3)_3Rh(AuPH_3)_3](H)_2^{2+}$ to the structure of a $RhAu_5$ cluster dication, $[(C_8H_9NC)_3Rh\{Au(PPh_3)\}_5]^{2+}$ ($C_8H_9CN$ = xylyl isocyanide), prepared recently by Mingos and co-workers.[33]

The minimum energy conformation for the monohydride $[(PH_3)_3Rh(AuPH_3)_3(H)^+$ is different. According to Figure 9b,

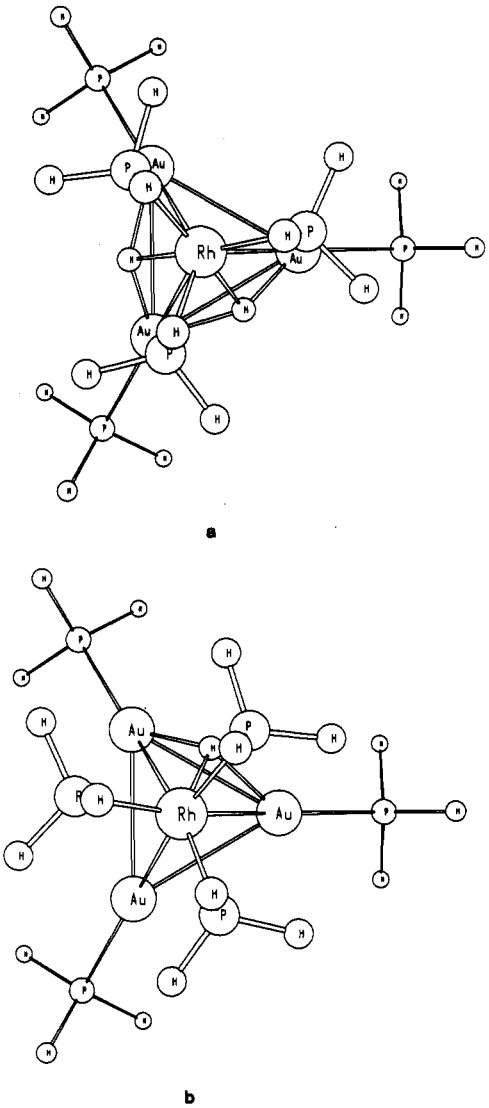


**Figure 9.** Minimum energy structures for (a) $[(PH_3)_3Rh(AuPH_3)_3](H)_2^{2+}$ as a model of **1** and (b) $[(PH_3)_3Rh(AuPH_3)_3](H)^+$ modeling **6** (top views as in Figure 8).

which shows the computed lowest energy $E = E(\alpha,\beta)$ structure, the $(PH_3)_3Rh$ tripod now adopts a staggered conformation with respect to the $Au_3$ triangle, but the hydrogen again sits in a face-bridging $\mu_3$ position.

The bonding in the "protonated" clusters with three or two hydrogens as bridges can now be described using the neutral $(PH_3)_3Rh(AuPH_3)_3$ core **8** from above and analyzing its interactions with the appropriate number of protons, i.e. with three or two empty 1s functions added to **8**. For simplicity we only give the corresponding interaction diagram for the $[(PH_3)_3Rh(AuPH_3)_3](H)_3^{3+}$ tris-cation, and we will furthermore describe this model for the idealized geometry **18**, with $C_{3v}$ symmetry, with all H's truly $\mu_3$ and with the $(PH_3)_3Rh$ fragment exactly eclipsed on top of the $(AuPH_3)_3$ subunit, instead of using the slightly distorted $C_3$ minimum structure of Figure 8. The general picture is of course not changed noticeably by this idealization.

At the left of Figure 10 are the filled valence levels of the $(PH_3)_3Rh(AuPH_3)_3$ cluster unit from Figure 6, $1a_1$, 1e, 2e, and $2a_1$ and the block of 15 d-type gold MOs. At the right the set of three empty group orbitals $a_1$ and e for an equilateral triangular arrangement of three protons interacting with **8** (H–H distances 2.35 Å, as in **18**), are given.[34] A strong interaction occurs with the symmetry-equivalent cluster HOMOs $2a_1$ and 2e (**11**–**13**,

(33) Bott, S. G.; Fleischer, H.; Leach, M.; Mingos, D. M. P.; Powell, H.; Watkin, D. J.; Watson, M. J. In press. We are grateful to Prof. D. M. P. Mingos for a preprint of this work, presented also at the IXth FECHEM Conference on Organometallic Chemistry, Heidelberg, Germany, July 1991. This cluster was also characterized by single-crystal X-ray diffraction. This mixed isocyanide/phosphine heteronuclear cluster has been described as a derivative of a Rh-centered $Au_{12}$ icosahedron by removing seven vertices from the icosahedral cage. Alternatively, however, in the context of our discussion of the dihydrido system **1** and as also mentioned by Mingos and co-workers, it can be viewed as a bicapped tetrahedron with two $Au(PPh_3)^+$ units capping two $RhAu_2$ faces of a $RhAu_3$ tetrahedron in a $\mu_3$-fashion, just as the protons of $[(PH_3)_3Rh(AuPH_3)_3](H)_2^{2+}$ in Figure 9a. Obviously the "$(C_8H_9CN)_3Rh$" fragment is electronically equivalent to the "(tripod)Rh" fragment of **1** and with "$(PH_3)_3Rh$" in our models making the Mingos cluster isoelectronic with **1** and supporting our conclusions for this system. Thus Mingos' compound and **1** provide, once again, nice examples of the isolobal analogy between $H^+$ and $AuPR_3^+$, leading to comparable structures. As found for **1**, the $RhAu_5$ cluster is fluxional in solution due to rapid intramolecular skeletal rearrangements.

(34) An equilateral triangular $(H)_3^{3+}$ unit of course has $D_{3h}$ symmetry, but for simplicity we use $C_{3v}$ symbols throughout.

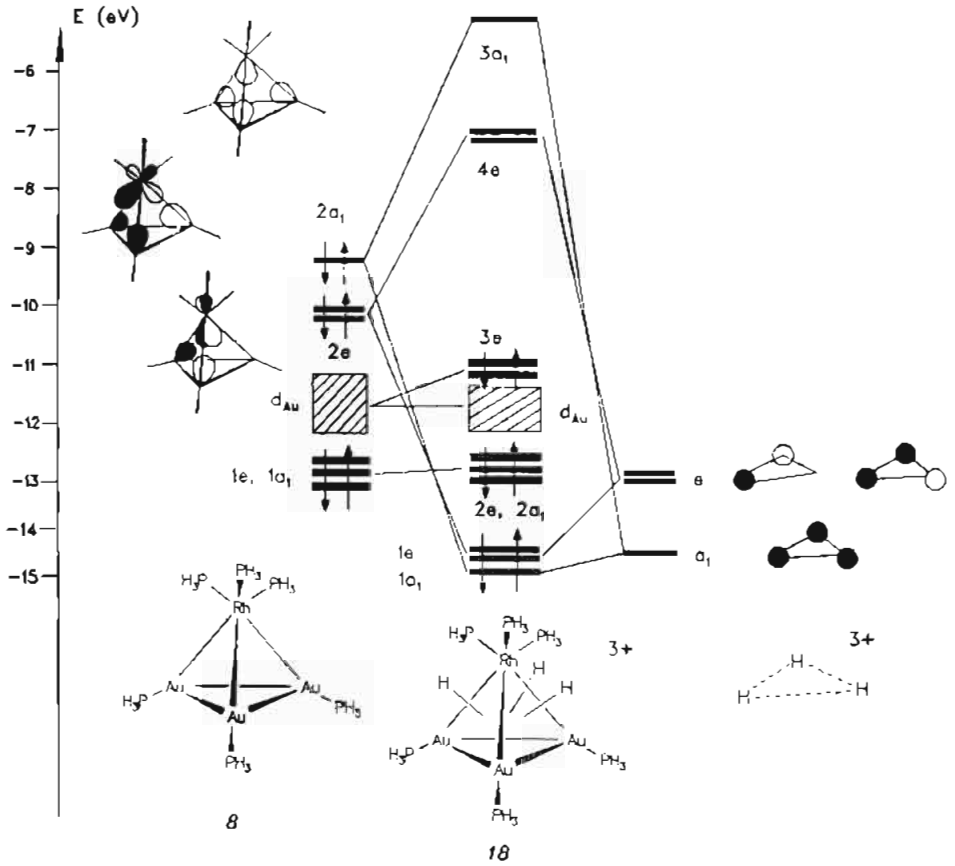


**Figure 10.** Interaction diagram between $(PH_3)_3Rh(AuPH_3)_3$, **8**, and three protons in $\mu_3$-positions over the $RhAu_3$ faces to show the valence electronic structure of $[(PH_3)Rh(AuPH_3)_3]H_3^{3+}$, **18**.

Figure 6) of **8**, leading to three low-lying Rh–H and Au–H bonding MOs $1a_1$ and 1e of $[(PH_3)_3Rh(AuPH_3)_3](H)_3^{3+}$.

Their antibonding counterparts $3a_1$ and 4e are at high energy. The $1a_1$ and 1e levels of fragment **8** as well as the 15 d-based, mainly Au-centered, MOs of **8** remain largely unaffected by protonation; only two levels (3e) of the original Au d-block are somewhat destabilized and emerge as the HOMO of $[(PH_3)_3Rh(AuPH_3)_3](H)_3^{3+}$. They are essentially still Au-centered MOs.

Overall there is a large transfer of electron density from the neutral cluster fragment **8** to the 1s linear combinations, depopulating the metal–metal bonding levels 2e and $2a_1$, thus reducing Rh–Au and Au–Au bonding but creating Rh–H and Au–H bonds. With as much as 1.21 electrons transferred from each 2e component of **8** to the two e-set levels of the former $(H)_3^{3+}$ moiety and 1.44 electrons going from $2a_1$ of **8** to $a_1$ of the three protons, the hydrogens in the cluster $[(PH_3)_3Rh(AuPH_3)_3](H)_3^{3+}$ become in fact hydridic, carrying a net charge of –0.288 each.

The overall bonding picture for the dihydride dication $[(PH_3)_3Rh(AuPH_3)_3](H)_2^{2+}$, which represents the real cluster **1**, is easily understood on the basis of Figure 10 as well. Instead of three now two 1s functions form an in-phase and out-of-phase combination and two fragment MOs for a $(H)_2^{2+}$ unit (similar to $\sigma$ and $\sigma^*$ of $H_2$).

For symmetry and overlap reasons then only $2a_1$ and one of the two components of 2e of **8** will interact strongly with the $(H)_2^{2+}$ orbital set. The other 2e member will stay put and will be the HOMO of a $[(PH_3)_3Rh(AuPH_3)_3](H)_2^{2+}$ cluster. Accordingly, only two metal–hydrogen bonding orbitals will appear at low energy, instead of the three levels $1a_1$ and 1e in Figure 10. These relationships are easily visualized by inspecting the orbital sketches of $2a_1$, $2e_s$, and $2e_a$ for **8** in **11**–**13** and in Figure 7, placing symmetric and antisymmetric 1s linear combinations above two cluster faces. This picture is confirmed by the calculations.

On the basis of Figure 10, it is also easy to discard the alternative structure for the dihydride system (and therefore for **1**), in which one H is interstitial and one is capping the $Au_3$ face, both sitting on the 3-fold molecular axis. This structure was tentatively discussed earlier as being also consistent with the highly symmetric solid-state structure of **1**. Obviously such a structure would not allow any interaction of either 1s linear combination shown in **20** with 2e of **8**, due to zero overlap with both components **12** and **13**.

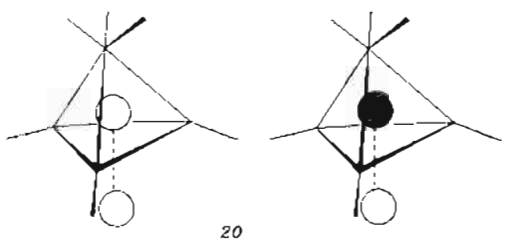

*20*

Model calculations indeed reveal 2e of **8** to remain energetically unaltered as the HOMO for an interstitial/$Au_3$-capping $(H)_2^{2+}$ location. Only $2a_1$ interacts with both 1s combinations, but the lowest total energy for this structure of $[(PH_3)_3Rh(AuPH_3)_3](H)_2^{2+}$ is around 3 eV higher than for the bis-$\mu_3$ isomer in Figure 9a. We will therefore not dwell upon this structural alternative any further.

Finally we turn to the monohydride $[(PH_3)_3Rh(AuPH_3)_3](H)^+$. Although in this case the real system **6** contains a $(CO)P_2Rh$ rather than a $P_3Rh$ cap, the calculations for the tris-$PH_3$ model predict a staggered orientation of the capping unit with respect to the $Au_3$ triangle, as found in the crystal structure of **6**. Again, however, a $\mu_3$-H position is preferred (Figure 9b). In the context of this work we did not test the effect of replacing one $PH_3$ by a CO ligand. This substitution might shift the hydrogen more toward $\mu_2$ than computed for $[(PH_3)_3Rh(AuPH_3)_3](H)^+$.

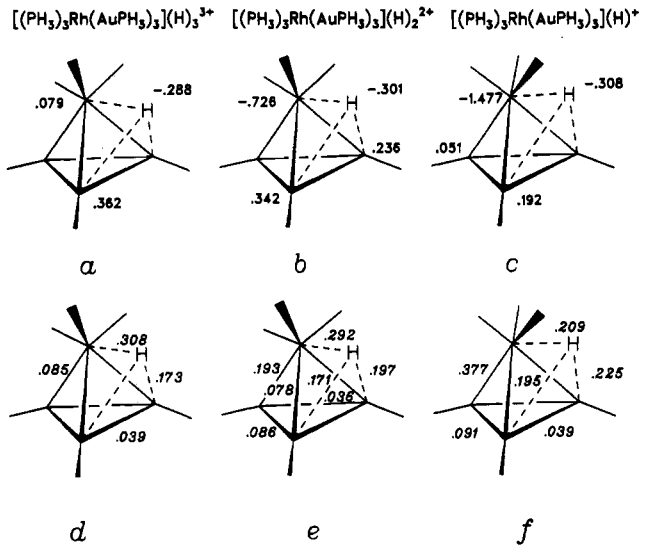


**Figure 11.** Atomic charges (a–c) and reduced overlap populations (d–f) for the trihydride $[(PH_3)_3Rh(AuPH_3)_3](H)_3^{3+}$, the $[(PH_3)_3Rh(AuPH_3)_3](H)_2^{2+}$ dihydride, and the monohydride $[(PH_3)_3Rh(AuPH_3)_3](H)^+$ for symmetrical $\mu_3$-positions of the bridging hydrides. Only one of the equivalent hydrides and one of two or three symmetry-equivalent numbers are given for the trihydride and dihydride cases.

We parenthetically note that in the experimental structure of **4** the location of the hydride was only deduced indirectly from the longer Rh–Au bond trans to the CO of the staggered $(CO)(PPh_3)_2Rh$ unit and that bending over to the other Au center of the $RhAu_2$ face was considered possible. The staggered orientation of the capping $Rh(PH_3)_3$ unit in $[(PH_3)_3Rh(AuPH_3)_3](H)^+$ and of $(CO)(PPh_3)_2Rh$ in **4** electronically reflects the fact that, in the monohydride case, i.e., in the monoprotonated $(PH_3)_3Rh(AuPH_3)_3$, a single H atom does not subtract a sufficient amount of Rh–Au bonding electron density to make direct Rh–Au bonding less important than Rh–H and H–Au bonding. Accordingly, a staggered orientation, as in the neutral, hydrogen-free **8**, with its direct Rh–Au bonds dominating, is favorable. The high negative charge of Rh of course makes the replacement of a phosphine by the acceptor CO a good choice and predicts much higher instability for monohydride clusters isoelectronic to **6** with phosphine ligands only at the capping $ML_3$ (e.g. for $[(triphos)Rh(AuPPh_3)_3](H)^+$, a hypothetical $[(triphos)Pd(AuPPH_3)_3](H)^{2+}$, etc.).

We can compare the trends of atomic charges and overlap populations (Mulliken population analysis) for the tri- and dihydride cation models and the monohydride with its staggered conformation. Again we take the numbers from calculations for idealized structures, fully eclipsed or staggered and symmetrically $\mu_3$-bridged. The data are displayed in Figure 11a–f and ought to be compared to those of **8** in **14a,b**. Only the values associated with the metals and hydrogens are given.[35]

In all three cases the bridging hydrogens take over approximately the same amount of net charge. In a sense we can associate this with the usual classification as cluster hydrides. The Rh atom becomes increasingly negative when the number of H-bridges decreases. The changes in net atomic charges are much smaller for the Au-centers, consistent with our earlier description of **8** and with Figure 10, where the dominant interaction occurs between the 1s functions at right and the Rh cap MOs. In simple terms, on going from $(PH_3)_3Rh(AuPH_3)_3$ to the cationic hydride clusters, we gradually substitute direct metal–metal bonding by metal–H, mainly Rh–H, bonding. Even for equidistant Rh–H and Au–H bonds (idealized $\mu_3$-H situation) there are strong Rh–H bonds but much weaker Au–H covalent interactions for the tri- and the dihydride cations. This corresponds to viewing them as intact octahedral $(PH_3)_3RhH_3$ and $(PH_3)_3RhH_2^-$ complexes, loosely bound to an $[(AuPH_3)_3]^{3+}$ unit (i.e. to three $AuPH_3^+$ cations with a weak mutual Au–Au attraction, induced by a partial population of their $a_1$ and e group orbitals). An eclipsed rather than staggered orientation of the $(PH_3)_3Rh$ cap with respect to the $Au_3$ unit maximizes Au–H interactions, while strong Rh–H bonds are retained.

In fragment **8** itself, where direct Rh–Au bonds are important, a staggered structure is preferred. It should be emphasized that the $\mu_3$- or nearly $\mu_3$-bonding of hydrides in the trihydride and the dihydride cations is quite different from the usual $\mu_3$ four-center bonding in other clusters.[36]

In contrast to the picture given by **21**, reflecting more or less equivalent bonds to three identical or comparable metal centers,

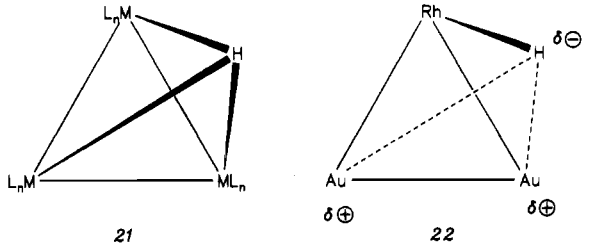


**22** is probably a more correct representation for the cases discussed here. Strongly "hydridic" hydrogen centers with covalent Rh–H bonds are only weakly linked to the two adjacent Au centers, with a large ionic contribution in these $H^-\cdots Au^+$ bonds. Thus equal (or nearly equal) M–H distances to Rh (Ru) and Au for a hydrogen on top of a $RhAu_3$ (or $RuAu_3$) cluster face do not indicate equal bond strengths or an electronically similar bonding situation toward all three metal centers as in standard $\mu_3$-$M_3H$ systems.

In the trihydride the Rh-bound H center is neighboring two Au atoms with a +0.362 charge; in the dihydride one Au carries an overall charge of +0.342 but the other is only +0.236, which makes the $\mu_3$-H (or quasi $\mu_3$-H) bonding situation in the latter more "normal". The real clusters, i.e. **1** and **3**, which we have so far modeled by the Rh systems $[(PH_3)_3Rh(AuPH_3)_3](H)_2^{2+}$ and $[(PH_3)_3Rh(AuPH_3)_3](H)_3^{3+}$, of course have different metal atoms as their (tripod)M cap, Rh and Ru, respectively.

We have not carried out similarly extensive calculations, optimizing H-positions also for $[(PH_3)_3Ru(AuPH_3)_3](H)_3^{2+}$ to model **3** more closely than done with the isoelectronic Rh trihydride tris-cation, but as Ru is generally assumed to be somewhat less electronegative than Rh,[37] it can be inferred that the $\mu_3$-hydrogen centers in isoelectronic Ru clusters get even more hydridic than in their Rh analogs, leading to an increasingly important polar contribution to Au–H bonding as shown in **21**. This was corroborated by a single point calculation for $[(PH_3)_3Ru(AuPH_3)](H)_3^{3+}$ with a geometry identical to that of **18** (–0.374 vs –0.288 charge on the three H centers).

Coming back to the data of Figure 11, we also note that going from the dihydride to the trihydride has a pronounced effect upon Au–Au bonding, consistent with our qualitative picture. For the bis-$\mu_3$-bridged system (Figure 11e), the averaged Au–Au overlap population is 0.052; for the trihydride (Figure 13d) it is reduced to 0.039, i.e. by around 25%, in accord with the experimentally observed Au–Au bond lengthening in the structure of **3** compared to **1**. In the dihydride model, the unique Au–Au bond, not involved in $\mu$-H bonding, is predicted to be stronger than the two others for obvious reasons and the unique Rh–Au bond bridged by both $\mu_3$-hydrogens is considerably weaker than the other two. The failure to observe this in the X-ray structure

(35) Charges and overlap populations of P atoms and M–P bonds behave consistently.

(36) Teller, R. G.; Bau, R. *Struct. Bonding* **1981**, *44*, 1.

(37) Nagle, J. K. *J. Am. Chem. Soc.* **1990**, *112*, 474 and references 1a–j, quoted therein.

of **1** is consistent with the above-mentioned possibility of 3-fold static disorder.

It is clear that the EH method employed in this study overestimates charge separation patterns[38] and cannot yield numerically accurate energetic or structural results. However, the qualitative bonding patterns and electronic structure descriptions gained from our model calculations, and the trends observed along the series of $[(PH_3)_3Rh(AuPH_3)_3](H)_n^{n+}$ model systems ($n$ = 1–3) representing **1**, **3**, **5**, and **6** are in accord with experimental findings and give a consistent picture of this important and fascinating class of gold clusters cations.

## Experimental Section

**Cluster Synthesis.** The clusters [(triphos)$RhH_2${$Au(PPh_3)_3$}]$(CF_3SO_3)_2$, **[1]**$(CF_3SO_3)_2$,[5] [(triphos)$IrH_2(PPh_3)_3](CF_3SO_3)_2$, **[2]**$(CF_3SO_3)$,[5] [(triphos)$RuH_3${$Au(PPh_3)$}$_3$][$PF_6$]$_2$, **[3]**[$PF_6$]$_2$,[6] and [(triphos)$RuH_2${$Au(PPh_3)$}$_3$][$PF_6$], **[7]**[$PF_6$][6] were prepared as described in the appropriate references. The corresponding clusters in which the H-ligand has been replaced by deuterium were prepared as described above starting from [$RhD_3$(triphos)], [$IrD_3$(triphos)], or [$RuD(BD_4)$(triphos)], respectively, prepared as described in the appropriate references, using the required deuterated solvents. The above mononuclear deuteride complexes were prepared as described for the corresponding hydrides starting from [$RhCl_3$(triphos)],[5] [$IrCl_3$(triphos)],[5] and [$Ru(CH_3CN)_3$(triphos)]$(CF_3SO_3)_2$[30] using the appropriate deuterated reagents and solvent.

**Infrared Spectra.** These were recorded on a Perkin-Elmer 1430 spectrophotometer in Nujol mulls, CsI pills, and $CH_2Cl_2$ solutions.

**Inelastic Neutron Scattering Experiments (IINS).** These were carried out at the Los Alamos Neutron Scattering Center (LANSCE) to determine the metal–hydrogen vibrational modes in **1** and **3**. In order to be able to distinguish the vibrational modes involving the M–H–M′ moiety (M = Ru, Rh; M′ = Au) from all other vibrational modes in these molecules (in particular those involving the hydrogen atoms of the ligands) a *sample difference* technique[40] had to be used. This technique is based on the fact that the incoherent neutron scattering cross section for hydrogen[41] is much greater than that of deuterium ($\sigma_{inc}$ = 79.91 and 2.04 barn, respectively). Vibrational modes involving deuterium atoms are therefore relatively difficult to observe by incoherent IINS in the presence of many hydrogens. Thus, the substraction of two experimental IINS spectra, i.e., that of the M–D–M′ analogue from that of the M–H–M′ compound, should leave only those peaks involving motion of the bridging hydrides, provided that any possible coupling of those modes to other vibrations of the ligands are negligible on the scale of the resolution of the IINS experiment. It is, therefore, unnecessary to use samples with deuterated triphos and phosphine ligands. However, the experiment requires a spectrometer with very high counting rates (and therefore modest energy resolution) in order to obtain reasonable statistics on the difference data set. The filter difference spectrometer[42] at LANSCE is well suited for this type of experiments given the very large detected solid angle and relaxed-energy resolution. In this spectrometer a pulsed "white" beam of neutrons is incident on the sample. The only neutrons detected, after scattering by the sample, are those whose energies (wavelength) have changed and fall below the Bragg "cut-off" (5.2 meV, λ ca. ~4 Å) of the Be filters which are placed between the sample and the detectors. This technique gives an effective final energy for the neutrons, while the incident energy is determined by the time of flight of the neutrons. The spectrometer can cover an energy range from 250 to 4000 $cm^{-1}$ with a resolution of 2–10% of the incident neutron energy.

Table VI. Atomic Parameters Used in the EH Calculations

| atom | orbital | $H_{ii}$ (eV) | $\zeta_1$ | $\zeta_2$ | $c_1$[a] | $c_2$[a] | ref |
|---|---|---|---|---|---|---|---|
| Rh | 5s | −8.09 | 2.135 | | | | 45 |
| | 5p | −4.57 | 2.100 | | | | |
| | 4d | −12.50 | 4.29 | 1.97 | 0.5807 | 0.5685 | |
| Au | 6s | −9.22 | 2.600 | | | | 46 |
| | 6p | −4.27 | 2.580 | | | | |
| | 5d | −11.85 | 6.16 | 2.73 | 0.64855 | 0.53946 | |
| P | 3s | −18.60 | 1.60 | | | | 43 |
| | 3p | −14.00 | 1.60 | | | | |
| H | 1s | −13.60 | 1.30 | | | | |

[a] Coefficients used in the double-ζ expansion.

Approximately 1.5 g of each complex (**1** and **3**, as well as their deuterium analogues) was sealed in cylindrical aluminum containers and maintained between 10 and 15 K. Counting times were approximately 30 h.

**Solid-State $^{31}$P NMR Spectra.** The solid-state $^{31}$P NMR spectra were recorded at 162.0 MHz on a Bruker AMX 400 spectrometer equipped for high-power experiments. Magic angle spinning at a rate of 12 kHz employing 4-mm o.d. rotors and the cross polarization technique with an 8-ms contact time were used. Typically 100–500 transients were accumulated, and the resulting FID was zero-filled and transformed by using resolution enhancement techniques.

**$^{197}$Au Mössbauer Spectra.** For the Mössbauer experiments, carried out at the Physics Department of the TU München, both the source and the absorber were cooled to 4.2 K in a liquid-He bath cryostat. The sources of $^{197}$Pt ($T_{1/2}$ = 19 h) in Pt metal were prepared by neutron irradiation of isotopically enriched $^{196}$Pt in the Munich Research Reactor. The Mössbauer spectra were least-squares fitted with superpositions of Lorentzian lines of equal width. The lines were grouped into two symmetrical doublets, with the quadrupole splitting, the isomer shift, and the relative intensity as free parameters. The isomer shifts in Table I are given relative to metallic gold. The errors quoted in Table I for isomer shifts, quadrupole splittings, and line widths are statistical ones only, to which an error of 0.5% for the velocity calibration has to be added.

**MO Calculations.** The molecular orbital calculations were of the extended Hückel type,[43] with atomic parameters specified in Table VI. A modified Wolfsberg–Helmholz formula for off-diagonal matrix elements was used throughout.[44] Idealized model geometries, adapted from the X-ray structure determination of **1**, were used.[5] Specific values were as follows. Distances (Å): Rh–Au = 2.695, Au–Au = 2.89, Rh–P = 2.31, Au–P = 2.26, P–H = 1.42, Rh–H = 1.80, Au–H (in $\mu_2$- and in idealized $\mu_3$-positions) = 1.80. $PH_3$ ligands: Local tetrahedral symmetry. $(PH_3)_3Rh(AuPH_3)_3$ core: $C_{3v}$ symmetry. Angles (deg): Au–Rh–P = 87, Rh–Au–P = 167.9. For the relative mutual $PH_3$ orientations, see the figures.

**Acknowledgment.** This work has benefited from the use of the facilities at the Manuel Lujan Jr. Neutron Scattering Center, a national facility funded as such by the Department of Energy, Office of Basic Energy Sciences. A.A. acknowledges support from NATO Grant 0068/85. The authors wish to thank Professor F. E. Wagner for the measurement of the $^{197}$Au Mössbauer measurements and their interpretation and Professor H. Schmidbaur for kindly arranging these measurements. Much appreciated by the authors were also the valid contributions of Dr. A. F. Williams for the interpretation of the $^{197}$Au Mössbauer chemical shifts and quadrupole splittings and of Prof. D. M. P. Mingos for making available the manuscript describing his $RhAu_5$ cluster prior to publication.

(38) This could have been partly circumvented by performing SCCC–EH calculations; however, the transparency in comparing trends within the series of models would be largely lost then.
(39) Rhodes, L. F.; Venanzi, L. M. *Inorg. Chem.* **1987**, *26*, 2692.
(40) Eckert, J. *Physica* **1986**, *136B*, 150.
(41) Sears, V. F. *Thermal Neutron Scattering Lengths and Cross-Sections for Condensed Matter Research*; Atomic Energy of Canada Ltd., Chalk River Nuclear Laboratories, Chalk River, Ont, Canada, 1984.
(42) Taylor, A. D.; Wood, E. J.; Goldstone, J. A.; Eckert, J. *Nucl. Instr. Methods* **1984**, *221*, 308.
(43) Hoffmann, R. *J. Chem. Phys.* **1963**, *39*, 1397.
(44) Ammeter, J. H.; Bürgi, H.-B.; Thibeault, J. C.; Hoffmann, R. *J. Am. Chem. Soc.* **1978**, *100*, 3686.
(45) Pinhas, A. R.; Albright, T. A.; Hofmann, P.; Hoffmann, R. *Helv. Chim. Acta* **1980**, *63*, 29.
(46) Evans, D. G.; Mingos, D. M. P. *J. Organomet. Chem.* **1985**, *295*, 389.